Quantum structure and dynamics for atom galleries

D. W. Vernooy* and H. J. Kimble
California Institute of Technology, Norman Bridge Laboratory of Physics, 12-33, Pasadena, California 91125
(Received 8 August 1996)

The bound state structure and dynamics for an atom trap formed from the whispering gallery modes (WGMs) of a dielectric microsphere are investigated. The coupling of the quantized internal and external atomic degrees of freedom plays a fundamental role in the quantum dynamics of this *atom gallery*. The radiative processes for a cold atom near a microsphere are modified due to the special symmetry of the atom gallery, the WGM mode structure, and the finite extent of the center-of-mass (c.m.) wave packet. Finally, interesting implications of the quantized c.m. for atomic matter waves and cavity QED with a quantum field are mentioned. [S1050-2947(97)01802-7]

PACS number(s): 42.50.Vk, 32.80.Pj, 33.80.Ps., 42.50.Hz

I. INTRODUCTION

Understanding atom–light-field interactions in a regime where the atoms are cold enough such that the center of mass (c.m.) degrees of freedom must be quantized has become very important in view of present experimental capabilities of sub-Doppler cooling and atom trapping. However, there exist few fully quantum calculations of the atomic c.m. dynamics in realistic three-dimensional (3D) configurations when dissipative processes must be taken into account [1].

The configuration of a three-level atom interacting with two oppositely detuned whispering gallery modes in a fused silica microsphere, termed an *atom gallery* in Ref. [2], is an ideal system in which to explore 3D atomic quantum dynamics because the relevant scale for the confining potential is of the order of the wavelength of light. The atom can behave as a free particle along a circumference of the surface of the sphere and still remain trapped in the two transverse directions. This suggests exciting possibilities for studies of matter wave resonance phenomena using cold atoms and for cavity QED in an extremely high Q resonator ($Q>10^9$) in a regime of strong coupling. Because experimental microsphere technology is rapidly advancing to the point where such experiments could actually be performed [3], it is important to explore in greater detail many of the the physical issues associated with such a system. Besides the advances in experimental aspects, several other groups have also performed calculations related to cavity QED effects in microsphere resonators [4,5].

The work reported here represents an important step forward in the understanding of the atom gallery. The first calculations of the 3D bound state structure and the associated c.m. wave functions for an atom in this trap have been performed for realistic experimental parameters in Sec. III. These c.m. states form a basis set which has then been used in Sec. IV in an attempt to understand the dynamics when an atom is allowed to evolve from a particular initial state. Next, in Sec. V these wave functions have been used to calculate the modified spontaneous emission rate for an atom occupying a particular eigenstate of the atom gallery. While it is well known that radiative processes are fundamentally modified for an atom outside of a dielectric sphere, previous calculations [6–9] have not included the quantum mechanical nature of the c.m. state. Finally, a few comments are made in Sec. VI about the possibilities for using these well-localized atomic wave packets for atomic resonance studies and also in cavity QED experiments.

II. THE ATOM GALLERY SYSTEM

In this section, we begin by describing the atom gallery system in terms of the optical fields, the atomic system, and the overall potential affecting the atomic c.m. Figure 1 shows the geometry of the atom gallery.

A. Whispering gallery modes

The excitation of the whispering gallery modes (WGMs) in a microsphere is accomplished experimentally by allowing the evanescent component of a focused Gaussian beam to meet the sphere at grazing incidence [10]. The classical electromagnetics problem of the resultant mode structure in the microsphere has been solved [11]. Two different polariza-

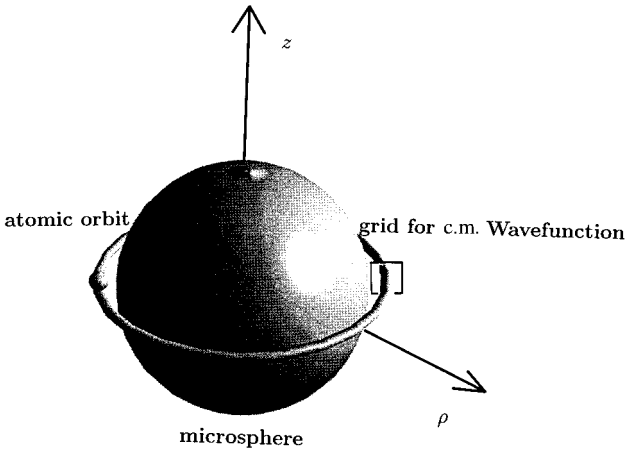

FIG. 1. The geometry of the atom gallery system is shown. The microsphere has a radius of $a=50$ μm and the grid on which the atomic c.m. wave functions are calculated has dimensions of 0.4 μm in the $\hat{\mathbf{e}}_\rho$ direction and 3 μm in the $\hat{\mathbf{e}}_z$ direction.

*Electronic address: dvernooy@cco.caltech.edu

tions, TE and TM, are allowed. The TE modes have no electric field amplitude in the radial ($\hat{\mathbf{e}}_r$) direction whereas the TM modes have a predominantly radial electric field vector. When solving the modal characteristic equations (see Appendix A 1 a) which are derived from enforcing the electromagnetic field boundary conditions at the surface of the sphere, one finds that allowed frequencies $\omega_{PL}^{\mathrm{TE}}$ and $\omega_{PL}^{\mathrm{TM}}$ are split far enough apart to be confident that only one polarization will be excited at any one time (the P and L indices will be explained below) and this is also realistic from an experimental point of view. Only modes of *electric type*, that is TM modes, will be considered here. The TM electric field inside the microsphere as a solution to the vector Helmholtz equation is written in (r,θ,ϕ) spherical polar coordinates as

$$E_r^{PLM}(r,\theta,\phi,t)=-L(L+1)\frac{j_L(k_{PL}^{\mathrm{TM}}r)}{k_{PL}^{\mathrm{TM}}r}\times P_L^M(\cos\theta)e^{iM\phi}e^{-i\omega_{PL}^{\mathrm{TM}}t},$$

$$E_\theta^{PLM}(r,\theta,\phi,t)=-\frac{[k_{PL}^{\mathrm{TM}}rj_L(k_{PL}^{\mathrm{TM}}r)]'}{k_{PL}^{\mathrm{TM}}r}\frac{\partial P_L^M(\cos\theta)}{\partial\theta}\times e^{iM\phi}e^{-i\omega_{PL}^{\mathrm{TM}}t},$$

$$E_\phi^{PLM}(r,\theta,\phi,t)=-\frac{iM}{\sin\theta}\frac{[k_{PL}^{\mathrm{TM}}rj_L(k_{PL}^{\mathrm{TM}}r)]'}{k_{PL}^{\mathrm{TM}}r},\times P_L^M(\cos\theta)e^{iM\phi}e^{-i\omega_{PL}^{\mathrm{TM}}t},\qquad(2.1)$$

where the P_L^M are associated Legendre polynomials and the j_L are spherical Bessel functions. The mode indices P and M are, respectively, the number of field maxima inside the sphere and the number of maxima in the $\hat{\mathbf{e}}_\phi$ direction. The mode number $L\approx k_{PL}^{\mathrm{TM}}a$ where a is the sphere radius. Note that k_{PL}^{TM} from here on is the magnitude of the wave vector-*inside* the sphere. WGMs are highly confined to the sphere equator and have $L\approx M$. The field outside the sphere is given by the above expressions in Eq. (2.1) with j_L replaced by the outgoing spherical Hankel function $h_L^{(1)}$ and k_{PL}^{TM} replaced by k_{PL}^{TM}/n where n is the index of refraction of the sphere.

B. Atomic system

The system considered is the one introduced by Mabuchi and Kimble [2], in which a three-level atom in a Vee configuration is driven by two oppositely detuned light fields which are simultaneously on resonance with WGMs in a fused silica microsphere as shown in Fig. 2. In particular, the state $|0\rangle\equiv|6S_{1/2}\rangle$ ground state in cesium is coupled to the $|1\rangle\equiv|6P_{1/2}\rangle$ level at 894.6 nm and the $|2\rangle\equiv|7P_{3/2}\rangle$ level at 455.6 nm by the two WGMs $\omega_{1,492}^{\mathrm{TM}}$ and $\omega_{1,996}^{\mathrm{TM}}$, respectively. The lower mode with mode numbers $(P_1,L_1,M_1)=(1,492,488)$ is detuned from the 894.6 nm transition by $\delta_1/2\pi=-2.38\times10^{12}$ Hz and the upper mode with mode numbers $(P_2,L_2,M_2)=(1,996,996)$ is detuned from the 455.6 nm transition by $\delta_2/2\pi=-2.20\times10^{12}$ Hz as determined from the characteristic equations which do not allow precisely symmetric detunings for these particular parameters. The fact that these modes are oppositely detuned from the atomic resonances allows them to form a potential minimum as discussed in the next subsection. The microsphere radius is $a=50.04$ μm and the index of refraction in the silica is $n=1.4518$ with a very small wavelength dependence [12]. Hyperfine structure in these levels is ignored for simplicity and clarity in the calculations.

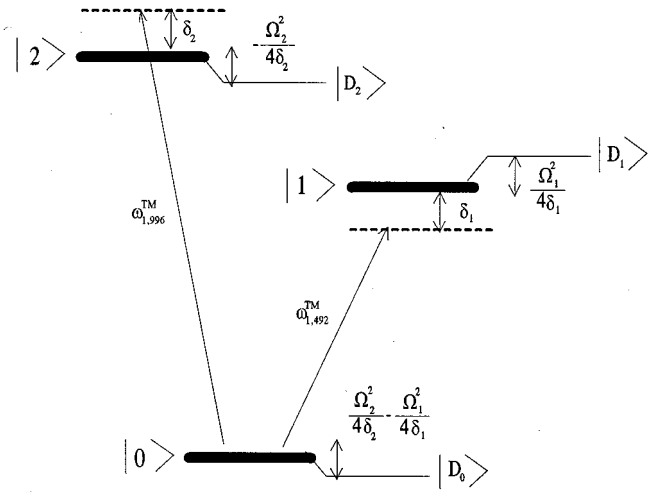

FIG. 2. The atomic system of [2] is a three-level atom in a Vee configuration (such as cesium) driven by two oppositely detuned whispering gallery modes (WGMs) of a dielectric microsphere. The Stark shift of the dressed ground state $|D_0\rangle$ consists of two opposing dipole forces which allows a potential minimum to form, as illustrated in Fig. 3 (and as in Ref. [2]). Values of the parameters for various potential wells are discussed in the text.

C. The potential

The bound state problem can be attacked in the following manner. First, the fields will be chosen such that the system forms a *far-off-resonance trap* (FORT) [13]. This means that the detunings $\delta_1/2\pi$ and $\delta_2/2\pi$ will be much greater in magnitude than both the field Rabi frequencies $\Omega_{1,2}(\mathbf{r})$ and the spontaneous decay rates $\Gamma_{1,2}(\mathbf{r})$. In this case the saturation parameters $s_{1,2}(\mathbf{r})\approx\Omega_{1,2}^2(\mathbf{r})/2\delta_{1,2}^2$ have a value much less than unity. For the 2 μK potential to be described below, $s_1\approx2\times10^{-6}$ and $s_2\approx1\times10^{-10}$. It is then valid to consider that the atom spends most of its time in the internal ground state. The light fields are coherent states with a large mean number of photons and can be treated classically. Therefore the quantized c.m. analysis proceeds by examining only the Stark shift of the ground dressed state of the atom-field system at a particular manifold of excitation number in order to determine the optical potential energy term. This term will be calculated explicitly later to be $\Omega_2^2(\mathbf{r})/4\delta_2-\Omega_1^2(\mathbf{r})/4\delta_1$. The force associated with this potential is known as the reactive force or dipole force [14]. A dissipative force due to spontaneous emission is not included in the potential but will become important when the dynamics of the system are discussed in Sec. IV. A van der Waals potential $V_{\mathrm{vdW}}(\mathbf{r})$ due to the interaction of the dipole with its image in the dielectric sphere is added to the optical dipole potential from the WGMs. The general functional form of $V_{\mathrm{vdW}}(\mathbf{r})$ is taken to be [15]

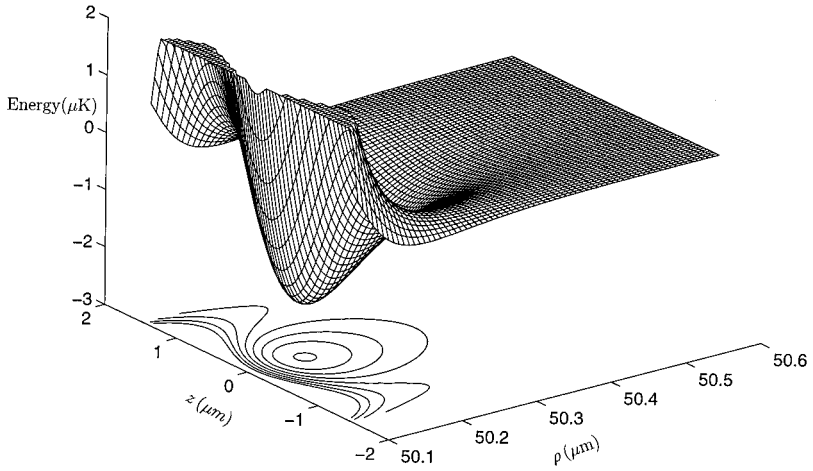

FIG. 3. The 3D 2 μK potential $V(\rho,z)$ as a function of ρ and z. The grid density shown is about two times as fine as was used in the dynamical calculations. A 40×40 grid was found to give good results in a reasonable length of time using the Lanczos algorithm [18] and FFT techniques.

$$V_{\mathrm{vdW}}(\mathbf{r})=-\frac{\alpha_{\mathrm{vdW}}}{(r-a)^3[1+k_{PL}(r-a)]}. \tag{2.2}$$

It is found that the correction term $k_{PL}(r-a)$ in the denominator, representing the Casimir-Polder regime, does not have a significant effect on the overall potential in the region in which the bound states are confined. Therefore the total potential is

$$V(\mathbf{r})=\frac{\Omega_2^2(\mathbf{r})}{4\delta_2}-\frac{\Omega_1^2(\mathbf{r})}{4\delta_1}-\frac{\alpha_{\mathrm{vdW}}}{(r-a)^3}. \tag{2.3}$$

The constant $\alpha_{\mathrm{vdW}}\approx 30$ Hz$(\mu\mathrm{m})^3$ has about 30% variation in the literature [15] between theory and experiment.

Using the definition of $\Omega_{1,2}(\mathbf{r})\equiv\mathbf{d}\cdot\mathbf{E}^{P_{1,2}L_{1,2}M_{1,2}}(\mathbf{r})$, we choose the overall magnitude of $\Omega_{1,2}(\mathbf{r})$ within the constraint of a small saturation parameter. After normalizing the field mode functions to a maximum value of unity which occurs inside the microsphere, the maximum value of the Rabi frequency in the well region is then chosen. The widths of the potential minima are found to be quite insensitive to changes in the parameters $\Omega_{1,2}(\mathbf{r})$ but the depth of the potential is readily adjustable. The largest well constructed has a depth of 95.6 μK with $\Omega_1^{\max}/2\pi=4\times10^{10}$ Hz and $\Omega_2^{\max}/2\pi=2\times10^8$ Hz occurring very close to the potential minimum at $\rho=r_0=50.141$ μm. Since the bound state structure of this potential turned out to be quite complicated (with 195 bound states) and hence not so useful in the dynamical calculations in Sec. IV, a shallower well of depth 2.06 μK was also considered whose bound states were calculated and used as a basis for calculations of the c.m. dynamics. This well had $\Omega_1^{\max}/2\pi=8\times10^9$ Hz and $\Omega_2^{\max}/2\pi=4\times10^7$ Hz. Since the potential is localized to a very small spread in θ about $\theta=\pi/2$, it is most convenient to use a (ρ,ϕ,z) cylindrical coordinate system. Figure 3 shows the potential in 3D. Figures 4(a) and 4(b) show sections through the potential well minimum at $z=0$, and $\rho=r_0=50.174$ μm.

III. BOUND STATE STRUCTURE FOR ATOM GALLERIES

A. The Schrödinger equation for the c.m.

The Schrödinger equation can be solved most easily numerically in cylindrical polar coordinates [16]. Since the potential is independent of ϕ, the trial wave function is taken as

$$\Psi_{\mathrm{c.m.}}^{\mathrm{atom}}(\rho,\phi,z,t)=\sum_{\lambda,m}c_{\lambda m}\frac{u_\lambda(\rho,z)}{\sqrt{\rho}}e^{im\phi}e^{-i(\tilde{E}_\lambda/\hbar)t}, \tag{3.1}$$

where the $c_{\lambda m}$ are expansion coefficients. The Schrödinger equation becomes

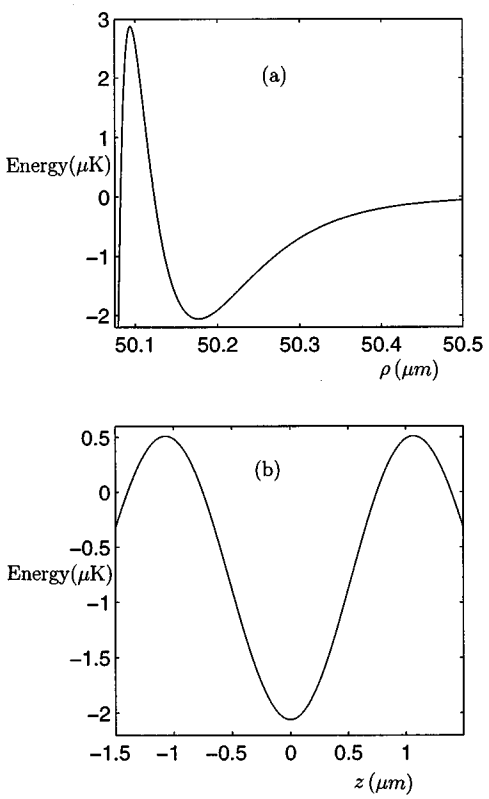

FIG. 4. In (a), the 2 μK potential is plotted as a function of ρ for fixed $z=0$ and in (b) the 2 μK potential is plotted as a function of z for fixed $\rho=r_0=50.174$ μm. The well has an extent of $\sim\lambda_{\mathrm{optical}}/2\pi\sim100$ nm (for $\lambda_{\mathrm{optical}}\sim900$ nm) in the $\hat{\mathbf{e}}_\rho$ direction centered on r_0 and an extent of ~1 μm in $\hat{\mathbf{e}}_z$.

$$\left[\begin{array}{c}\dfrac{\partial^2}{\partial\rho^2}+\dfrac{\partial^2}{\partial z^2}\\ -\dfrac{2m_c}{\hbar^2}\left[V(\rho,z)-\dfrac{\hbar^2}{2m_c}\left(\dfrac{\frac{1}{4}-m^2}{\rho^2}\right)\right]-\widetilde{E}_\lambda\end{array}\right]u_\lambda(\rho,z)=0, \tag{3.2}$$

where m_c is the mass of the cesium atom and m is the quantum number associated with the $\hat{\mathbf{e}}_\phi$ direction. The index λ is for the set of solutions to Eq. (3.2). There are two important points about this equation. First, the effective potential contains a centrifugal term $E_c=-(\hbar^2/2m_c)[(\frac{1}{4}-m^2)/\rho^2]$. Now, from the preceding discussion of the potential and Fig. 4(a), it is clear that the potential itself contains a repulsive barrier at $\rho_1=50.1$ μm and is effectively zero by $\rho_2=50.5$ μm. Likewise, it forms a well in the z direction for $|z|<1.5$ μm as can be seen from Fig. 4(b). One can calculate a tunneling probability for the finite barrier height at ρ_1 and can show the error made by ignoring it is negligibly small. Therefore the bound state solutions must be confined to the region 50.1 μm$<\rho<50.4$ μm and -1.5 μm$<z<1.5$ μm. The boundary condition that $\Psi^{\text{atom}}_{\text{c.m.}}(\mathbf{r})=0$ outside this region is imposed and any evanescent tail to the wave function is ignored.

The variation of the centrifugal term across the allowed region is also neglected because the ρ variation is so slight and to an excellent approximation it can be treated as a global shift in the c.m. energy of the atom. The bound states can then be calculated by ignoring the centrifugal term altogether. There is a limit to this approximation: when the centrifugal force is large enough to overcome the trapping force, the atom will no longer be trapped. The trapping force is the gradient of the trapping potential. Using the asymptotic form of the spherical Hankel function, we find that this force is $\approx 2k^{\text{TM}}_{P_1L_1}V_0$ in the $-\hat{\mathbf{e}}_\rho$ direction, where V_0 is the trap depth. Equating this to the centripetal force gives $m_{\max}\approx\sqrt{2k_{P_1L_1}V_0m_ca^3/\hbar^2}$. For a trap depth of $V_0=2$ μK this gives $m_{\max}\approx 30\,000$ for a total energy of $E_{\text{tot}}=700$ μK. Precooling the atoms before loading such a trap would get them well below this limit and therefore centrifugal heating is *not* a practical limitation as also stated in Ref. [2] and found in Ref. [17].

The second point to be emphasized is that the atom is trapped in the $\hat{\mathbf{e}}_\rho$ and $\hat{\mathbf{e}}_z$ directions but is a free particle in the $\hat{\mathbf{e}}_\phi$ direction, so the situation is somewhat analogous to a 1D electron. In the case of the atom gallery, the energy in the $\hat{\mathbf{e}}_\phi$ direction can be much greater than the depth of the trap itself and yet the atom can remain trapped. For the rest of this work, the *total* atomic energy is referred to as E_{tot}. This is a sum of the centrifugal energy $E_c=\hbar^2m^2/2m_ca^2$ and the c.m. energy $E_{\text{c.m.}}$ to be defined below. In practice, the former dominates this sum. Hence, $E_{\text{c.m.}}<0$ and $E_{\text{tot}}<k^{\text{TM}}_{P_1L_1}aV_0$ are the conditions for a trapped atom.

A little bit about the structure of the solutions can be guessed before actually solving this equation. First, as the energy of the atom in the $\hat{\mathbf{e}}_\rho$ and $\hat{\mathbf{e}}_z$ directions increases, the probability distribution is expected to shift to larger and larger ρ and away from $z=0$. With $E_\lambda=\widetilde{E}_\lambda-\hbar^2m^2/2m_ca^2$ (or $E_{\text{c.m.}}=E_{\text{tot}}-E_c$) defined as *only* the sum of the ρ and z energies, the Schrödinger equation, Eq. (3.2), becomes

$$\left[\frac{\partial^2}{\partial\rho^2}+\frac{\partial^2}{\partial z^2}-\frac{2m_c}{\hbar^2}V(\rho,z)-E_\lambda\right]u_\lambda(\rho,z)=0. \tag{3.3}$$

As E_λ becomes more positive for the higher lying bound states, the distribution moves closer to the second classical turning point at ρ_2. States with $E_\lambda>0$ but less than the barrier height at ρ_1 will become approximately free waves. This sort of structure should start to become visible in the higher bound states. Atoms with E_λ greater than the barrier at ρ_1 will crash into the sphere surface due to the van der Waals potential.

Finally, by analogy with an anisotropic 2D rectangular well, the different trap sizes in the two directions will lead to a series of states associated with increasing numbers of nodes towards the higher bound energies. Since the trap is much tighter in the $\hat{\mathbf{e}}_\rho$ direction than in the $\hat{\mathbf{e}}_z$ direction, the lowest states are expected to sequentially increase the numbers of nodes in the $\hat{\mathbf{e}}_\rho$ direction and the appearance of a state with a node in the $\hat{\mathbf{e}}_z$ direction will be higher up the ladder.

The solution of Eq. (3.3) is now fairly straightforward [16]. The use of a sine series representation (see Appendix A 2 a) for $u_\lambda(\rho,z)$ means the boundary conditions will automatically be satisfied. By using a discretized grid of points in the region of interest, Eq. (3.3) can be rewritten as an eigenvalue problem for a matrix whose dimensions are proportional to the grid size. Such a problem can be solved efficiently using the Lanczos algorithm [18] and fast Fourier transform (FFT) techniques.

B. Bound state c.m. wave function solutions and eigenvalue spectra

Results for the 95 μK well are shown in Figs. 5 and 6. Figure 5(a) shows the c.m. ground state $u_{\lambda=1}(\rho,z)$ and Fig. 6(b) shows the energy spectrum $E_{\text{c.m.}}(\lambda)$. There are 195 bound states. The spectrum of the first 25 bound states is overlaid on the potential in Fig. 6(a) showing that the lowest two states are split by an energy of 1.19 μK which is somewhat greater than both the recoil energy of 350 nK for the 456 nm transition and the recoil energy of 90 nK for the 894 nm transition. Cooling the atom to this c.m. ground state would result in a c.m. energy $E_{\text{c.m.}}=-89.5$ μK in the 95.6 μK well with a kinetic energy in the trapped $\hat{\mathbf{e}}_\rho$ and $\hat{\mathbf{e}}_z$ directions of 6.1 μK. The states $\lambda=16$ with $E_{\lambda=16}=-64.23$ μK and $\lambda=77$ with $E_{\lambda=77}=-27.84$ μK are shown in Figs. 5(b) and 5(c), respectively. Modes can be labeled by the number of nodes in the $\hat{\mathbf{e}}_\rho$ and the $\hat{\mathbf{e}}_z$ directions.

The results for the 2 μK well are summarized in Figs. 7 and 8. There are exactly 13 bound states. The first nine states correspond to successive increases by one in the number of radial lobes; it is not until the $\lambda=10$ state shown in Fig. 8(a) that structure in the $\hat{\mathbf{e}}_z$ direction appears. The *shape* of the potentials in the two directions is very important in determining bound state structure because this spectroscopic sequence is *not* what one would expect in the limit of a 2D rectangular well of the same dimensions. Figures 8(b) and 8(c) show the bound states $\lambda=12$ and $\lambda=13$, respectively. It is reassuring that these states are also confined fairly well inside the potential, which justifies ignoring the small probability outside the region of interest by enforcing boundary conditions.

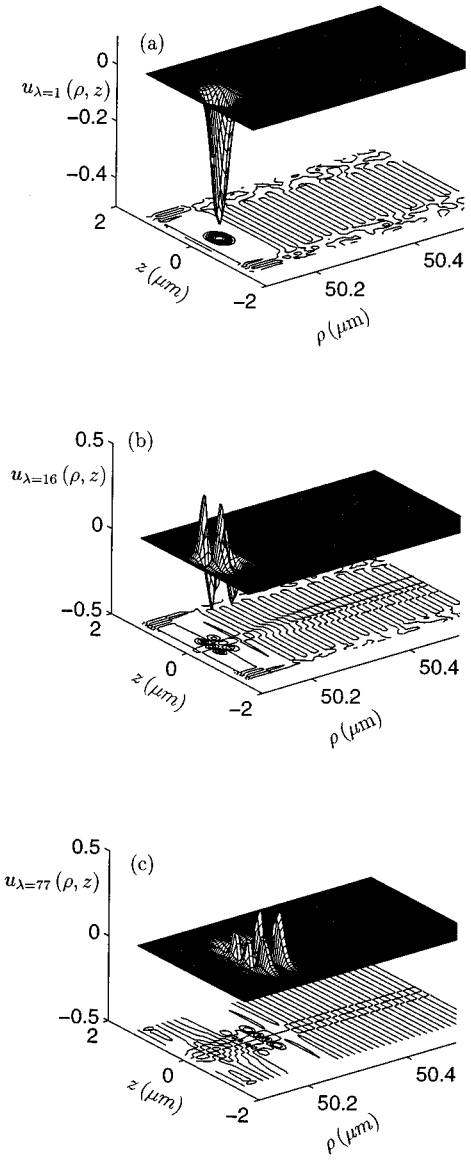

FIG. 5. The $\lambda=1$ bound state of the 95 μK potential is shown in (a), the $\lambda=16$ state in (b), and the $\lambda=77$ state in (c). These states can be labeled by the number of nodes in the $\hat{\mathbf{e}}_\rho$ and $\hat{\mathbf{e}}_z$ directions.

As shown in the spectrum in Fig. 9, the ground state is split from the first excited state by 185 nK. Evidently, there are also near degeneracies between the modes with excitations in the two directions, such as for the sets $\{\lambda_9,\lambda_{10}\}$ and $\{\lambda_{12},\lambda_{13}\}$. Such near degeneracies are also responsible for the thicker lines in Fig. 6(a) for the 95 μK well.

The calculations in Sec. IV on the dynamics of an atom trapped around a sphere will be done using the 2 μK potential since 13 bound states is a computationally reasonable number to deal with. A 1 μK well initially considered had only one bound state.

A second expansion of the wave function in a spherical geometry was attempted using

$$\Psi^{\text{atom}}_{\text{c.m.}}(\mathbf{r},t)=\sum_{\lambda,m}\sum_{l\geqslant|m|} d_{\lambda lm}v_\lambda(r)P_l^m(\cos\theta)e^{im\phi}e^{-i(E_\lambda/\hbar)t}, \tag{3.4}$$

with $\mathbf{r}=(r,\theta,\phi)$ in order to better understand the properties

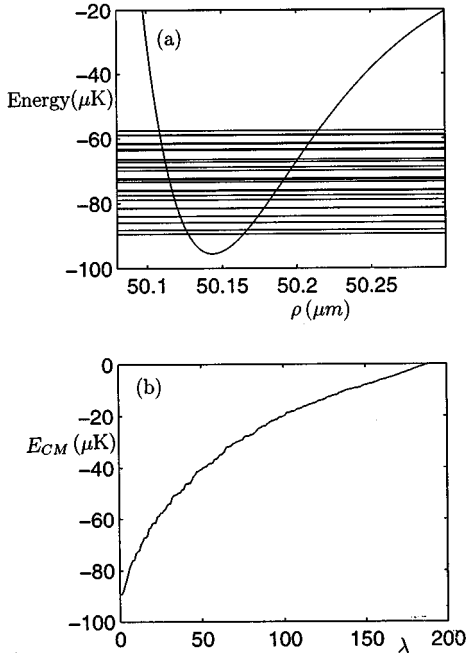

FIG. 6. The first 25 ($\lambda=1,\ldots,25$) bound state energy levels of the 95 μK potential overlaid on the potential as a function of ρ plotted for fixed $z=0$ are shown in (a). The kinetic energy of the $\lambda=1$ state is $\sim$6.1 μK and the energy splitting of the first two bound states is 1.2 μK. In (b), the bound state energy spectrum for the 195 bound states of the 95 μK potential are shown. The last few eigenvalues ($160<\lambda<195$) have non-negligible error associated with them. This can be fixed by more iterations of the Lanczos algorithm at the cost of significantly more computational time required [18].

of the bound states. It was found that the sum $\Sigma_{l\geqslant|m|}$ required only one or two terms to reconstruct faithfully the bound states as long as m was large. This is because the spherical harmonics (and associated Legendre polynomials) with $l\sim m$ and m large are very closely confined to the equator [19]. Large m is not a problem since even a moderate $m\sim100$ corresponds to a very cold atom with total energy $E_{\text{tot}}\sim180$ nK. The fact that this reconstruction converges so well with very few angular components is confirmation that the c.m. wave functions are extremely well localized.

IV. QUANTUM DYNAMICS OF THE ATOM-MICROSPHERE SYSTEM

A. Description of the wave function

The wave function which must be considered in a complete quantum description of the system is the following tensor product:

$$|\Psi^{\text{system}}_{\text{tot}}\rangle=|\Psi^{\text{atom}}_{\text{c.m.}}\rangle\otimes|\Psi^{\text{atom}}_{\text{int}}\rangle\otimes|\Psi^{\text{microsphere}}_{\text{field}}\rangle, \tag{4.1}$$

with $\langle\mathbf{r},t|\Psi^{\text{atom}}_{\text{c.m.}}\rangle$ given by

$$\Psi^{\text{atom}}_{\text{c.m.}}(\rho,\phi,z,t)=\sum_{\lambda,m} c_{\lambda m}(t)\frac{u_\lambda(\rho,z)}{\sqrt{\rho}}e^{im\phi}, \tag{4.2}$$

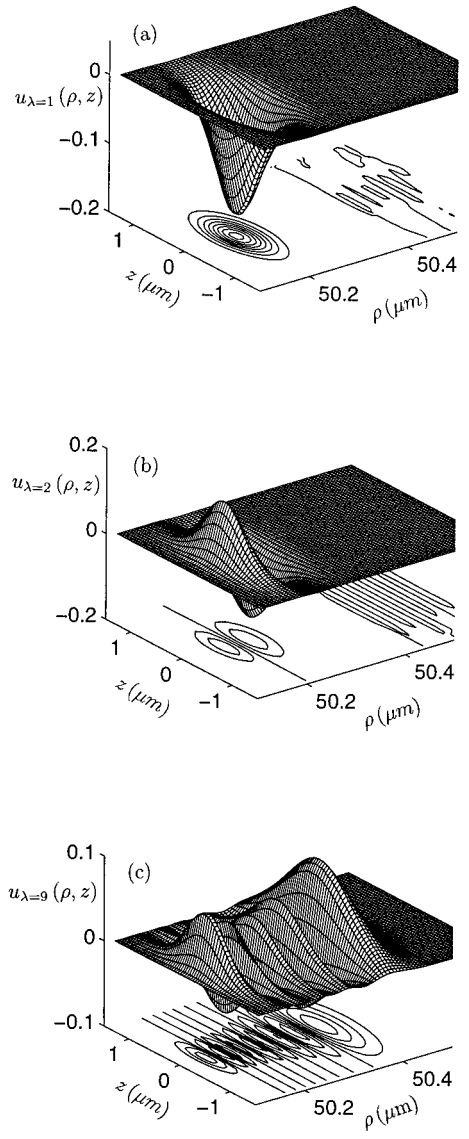

FIG. 7. In (a) the $\lambda=1$ bound state is shown for the 2 μK potential. Note that it has a significantly greater spatial extent than the corresponding c.m. state for the 95 μK potential in Fig. 5(a). The number of extrema in the $\hat{\mathbf{e}}_\rho$ direction increases with λ [e.g., in (b) $\lambda=2$ has two lobes] until the $\lambda=9$ bound state in (c).

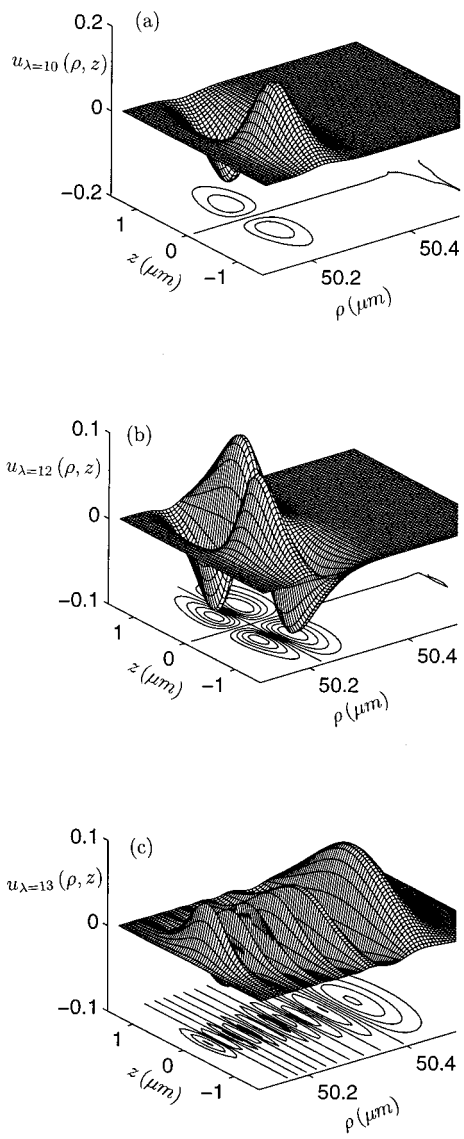

FIG. 8. The $\lambda=10$ bound state of the 2 μK potential in (a) shows the first excited state in the $\hat{\mathbf{e}}_z$ direction, which is almost degenerate with the $\lambda=9$ state. In (b) and (c), the states $\lambda=12,13$ are shown, respectively.

with $\mathbf{r}$ as the c.m. position of the atom and $\lambda=1,...,13$ as calculated in the preceding section using the 2 μK well. Since we restricted this expansion to include only the bound state solutions (i.e., not the unbound solutions), it is not a complete expansion for any arbitrary c.m. wave function but should be a good approximation for the lower bound states. For example, restricting the analysis to the dynamics of the bound state with $\lambda=1$ and $c_{\lambda m}(t=0)=\delta_{\lambda,1}$, it is expected that the other $c_{\lambda m}$ with $\lambda\neq 1$ will stay small until the atom becomes appreciably heated out of the ground state. At the other extreme, the expansion of Eq. (4.2) would not be valid in computing the evolution of the state with $\lambda=13$ because this state will very quickly become a state with some large probability to be in the continuum.

Turning next to the internal state, we have that $\langle\mathbf{R}|\Psi_{\text{int}}^{\text{atom}}\rangle$ is given by

$$\langle\mathbf{R}|\Psi_{\text{int}}^{\text{atom}}\rangle=\sum_i b_i\langle\mathbf{R}|i\rangle, \tag{4.3}$$

where $\mathbf{R}$ is the position of the electron with respect to the atomic c.m. and $\{|i\rangle\}$ is the set of bare internal levels of the cesium atom. Explicitly, $|0\rangle=|6S_{1/2}\rangle$, $|1\rangle=|6P_{1/2}\rangle$, and $|2\rangle=|7P_{3/2}\rangle$, which again are taken to be nondegenerate. These levels need to be reexpressed in terms of the dressed levels $\{|D_i\rangle\}$.

The easiest way to do this is to consider the following eigenstates and uncoupled energies of the state manifold:

$$|\Psi_{\text{int}}^{\text{atom}}\rangle\otimes|\Psi_{\text{field}}^{\text{microsphere}}\rangle$$
$$=\{|i\rangle\}\otimes|n_{P_1L_1M_1}^{\text{TM}}\equiv n_1\rangle\otimes|n_{P_2L_2M_2}^{\text{TM}}\equiv n_2\rangle, \tag{4.4}$$

with quanta distributed as follows:

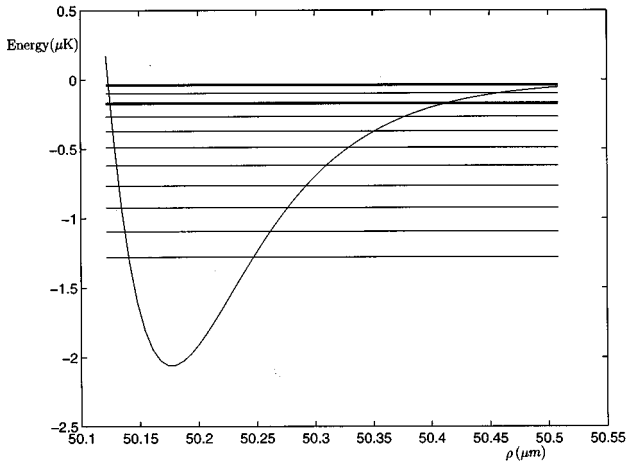

FIG. 9. The 13 bound state energy levels of the 2 μK potential overlaid on the potential as a function of ρ plotted for fixed $z=0$. The $\lambda=1$ and $\lambda=2$ c.m. energy ($E_{\text{c.m.}}$) splitting is 180 nK. The $\lambda=1$ bound state kinetic energy here is $\sim$730 nK.

$$\left\{\begin{array}{c}|0,n_1,n_2\rangle\\ |1,n_1-1,n_2\rangle\\ |2,n_1,n_2-1\rangle\end{array}\right\}\leftrightarrow\left(\begin{array}{c}E_0=n_1\omega_1+n_2\omega_2\\ E_1=(n_1-1)\omega_1+n_2\omega_2+\delta_1\\ E_2=n_1\omega_1+(n_2-1)\omega_2-\delta_2\end{array}\right). \tag{4.5}$$

The coupling Hamiltonian (in the rotating wave approximation) is written

$$H^{\text{interaction}}_{\text{field}\otimes\text{ int}}=\sum_{j=1,2}\frac{1}{2}(a_jR_j^\dagger+a_j^\dagger R_j)\Omega_j(\mathbf{r}), \tag{4.6}$$

with a_j as a field mode annihilation operator and R_j as an atomic lowering operator for the three-level system. The total Hamiltonian, in a frame rotating at $\omega_1+\omega_2$, and ignoring mode decay and spontaneous emission in the limit of large detunings and small saturation parameters, is

$$H^{\text{tot}}_{\text{field}\otimes\text{ int}}=\left(\begin{array}{ccc}0&\frac{\Omega_1(\mathbf{r})}{2}&\frac{\Omega_2(\mathbf{r})}{2}\\ \frac{\Omega_1(\mathbf{r})}{2}&\delta_1&0\\ \frac{\Omega_2(\mathbf{r})}{2}&0&\delta_2\end{array}\right). \tag{4.7}$$

Diagonalizing this gives the following transformation, which is valid to first order in the saturation parameters $s_{1,2}(\mathbf{r})$:

$$\left(\begin{array}{c}|D_0\rangle\\ |D_1\rangle\\ |D_2\rangle\end{array}\right)=\mathcal{T}(\mathbf{r})\left(\begin{array}{c}|0\rangle\\ |1\rangle\\ |2\rangle\end{array}\right)+O(s_{1,2}^2(\mathbf{r})), \tag{4.8}$$

where the transformation matrix $\mathcal{T}(\mathbf{r})$ is defined as

$$\mathcal{T}(\mathbf{r})\equiv\left(\begin{array}{ccc}1-\frac{\Omega_1^2(\mathbf{r})}{8\delta_1}-\frac{\Omega_2^2(\mathbf{r})}{8\delta_2}&-\frac{\Omega_1(\mathbf{r})}{2\delta_1}&\frac{\Omega_2(\mathbf{r})}{2\delta_2}\\ \frac{\Omega_1(\mathbf{r})}{2\delta_1}&1-\frac{\Omega_1^2(\mathbf{r})}{8\delta_1}&0\\ -\frac{\Omega_2(\mathbf{r})}{2\delta_2}&0&1-\frac{\Omega_2^2(\mathbf{r})}{8\delta_2}\end{array}\right). \tag{4.9}$$

The corresponding Stark shifts are

$$\left(\begin{array}{c}\delta E_0\\ \delta E_1\\ \delta E_2\end{array}\right)=\left(\begin{array}{c}\frac{\Omega_2^2(\mathbf{r})}{4\delta_2}-\frac{\Omega_1^2(\mathbf{r})}{4\delta_1}\\ \frac{\Omega_1^2(\mathbf{r})}{4\delta_1}\\ -\frac{\Omega_2^2(\mathbf{r})}{4\delta_2}\end{array}\right). \tag{4.10}$$

Note that δE_0 was used in the preceding calculation of the potential and it is a trapping potential. However, small amounts of population in $|D_1\rangle$ and $|D_2\rangle$ are affected by attractive and repulsive forces, respectively. Both of these cause dipole heating which will be investigated in detail in Sec. IV B below. The heating mechanisms for the atom cause the internal state to become *entangled* with the external state so that the wave function $\langle\mathbf{r},t|\Psi^{\text{atom}}_{\text{c.m.}}\rangle\otimes|\Psi^{\text{atom}}_{\text{int}}\rangle$ must be represented as the following spinor in the bare state basis:

$$\begin{aligned}\langle\mathbf{r},t|\Psi^{\text{system}}_{\text{tot}}\rangle&=\langle\mathbf{r},t|\Psi^{\text{atom}}_{\text{c.m.}}\rangle\otimes|\Psi^{\text{atom}}_{\text{int}}\rangle\\ &=\left(\begin{array}{c}\sum_{\lambda,m}c_{\lambda m}(t)\frac{u_\lambda(\rho,z)}{\sqrt{\rho}}e^{im\phi}\\ \sum_{\lambda',m}b_{\lambda' m}(t)\frac{u_{\lambda'}(\rho,z)}{\sqrt{\rho}}e^{im\phi}\\ \sum_{\lambda'',m}d_{\lambda'' m}(t)\frac{u_{\lambda''}(\rho,z)}{\sqrt{\rho}}e^{im\phi}\end{array}\right).\end{aligned} \tag{4.11}$$

The three entries correspond to different external state expansions for each internal state, or to an entanglement of the external and internal states and the $c_{\lambda m}(t)$, $b_{\lambda' m}(t)$, and $d_{\lambda'' m}(t)$ are simply coefficients for these three different expansions associated with the bare internal states $|0\rangle$, $|1\rangle$, and $|2\rangle$, respectively. For the purposes of the computation, this is stored as a $39\times r$ matrix where r is the number of m values involved in Σ_m and the 39 corresponds to $\lambda=1,\ldots,13$ for each of the three internal states.

A quantum description of the field modes on resonance with the cavity is not necessary because the photon numbers are very large ($\langle n_{1,2}\rangle\sim10^6$, see Appendix A 4) so that a loss or a gain of a photon is not an issue to these dynamics. It should also be noted that even for small photon numbers, the high quality factors expected in these microspheres mean the cavity mode decay rates $\kappa_{1,2}=\kappa^{\text{TM}}_{P_1L_1,P_2L_2}$ can be much smaller than the rate scales governing the dynamics ([10], and Appendix A 1 b). Therefore the field component in the total quantum wave function in Eq. (4.1) is considered to be

the coherent state $|\Psi_{\text{field}}^{\text{microsphere}}\rangle = |\alpha_{P_1 L_1 M_1}\rangle \otimes |\alpha_{P_2 L_2 M_2}\rangle$, which is taken to be constant for all times.

B. Heating of the atomic c.m. in an atom gallery

There are two main mechanisms for the heating of an atom initially in a c.m. bound state [14]. The first is fluctuations in the dipole forces. Even though the internal ground dressed state will be affected by a trapping potential, an atom prepared in this state will also occupy the other two dressed states during the normal course of its evolution, albeit with greatly reduced probability. These other two states are not in the same effective trapping potential but are in purely repulsive or attractive potentials. This can be seen from the expressions for the Stark shifts of these other two levels in Eq. (4.10). Note, however, that the atomic evolution still remains unitary for dipole heating.

The second heating process is recoil heating after a spontaneous emission event. The atomic c.m. will receive a kick due to conservation of momentum in the emission of a photon, with each kick tending to change the energy of the atom by the atomic recoil energy $\sim \hbar^2 k^2/2m$. Section V will be devoted to a more complete understanding of the spontaneous emission process but it must be mentioned now that the effect of this process on the c.m. dynamics of the trap is not important. The first reason is obvious: the trap is a FORT and hence the average time between spontaneous decays is $\Delta t_{\text{emission}} \sim 1/s\Gamma$ where s is the saturation parameter and Γ is the spontaneous decay rate. Even though Γ is modified somewhat from its free space value (Sec. V B), $\Delta t_{\text{emission}} \sim 20$ ms which turns out to be of the order of τ_{heating}, the trap lifetime. The processes which tend to limit the trap lifetime will be discussed below in Sec. IV C. The second reason is rather more subtle. Momentum conservation in spontaneous decay dictates that the orbital angular momentum carried away by the photon will affect the orbital angular momentum of the atom (quantum number m) and hence the energy primarily affected by the atomic recoil is the centrifugal energy E_c. As described earlier, changes in E_c caused by typical angular momenta $\sim M\hbar$ from a WGM of orbital angular momentum $L \sim M$ will not cause significant trap heating. Therefore we will ignore spontaneous emission in the atom gallery dynamics.

The wave function is evolved according to

$$|\Psi_{\text{tot}}^{\text{system}}(t)\rangle = e^{-iHt}|\Psi_{\text{tot}}^{\text{system}}(0)\rangle, \tag{4.12}$$

where H, in a basis given by $\{|u_\lambda\rangle\} \otimes \{|i\rangle\}$, is given by

$$H = E_{\text{kin}} + \mathcal{T}^T(\mathbf{r}) E_{\text{pot}} \mathcal{T}(\mathbf{r}), \tag{4.13}$$

with

$$E_{\text{kin}} = \begin{pmatrix} \dfrac{\mathbf{p}^2}{2m} & 0 & 0 \\ 0 & \dfrac{\mathbf{p}^2}{2m} & 0 \\ 0 & 0 & \dfrac{\mathbf{p}^2}{2m} \end{pmatrix} \tag{4.14}$$

in the bare basis and

$$E_{\text{pot}} = \begin{pmatrix} \dfrac{\Omega_2^2(\mathbf{r})}{4\delta_2} - \dfrac{\Omega_1^2(\mathbf{r})}{4\delta_1} & 0 & 0 \\ 0 & \dfrac{\Omega_1^2(\mathbf{r})}{4\delta_1} & 0 \\ 0 & 0 & -\dfrac{\Omega_2^2(\mathbf{r})}{4\delta_2} \end{pmatrix} - \frac{\alpha_{\text{vdW}}}{(r-a)^3}\mathbb{1} \tag{4.15}$$

in the dressed basis [$\mathcal{T}(\mathbf{r})$ in Eq. (4.13) is used to transform between bases]. In order that the aforementioned approximation concerning the completeness of the c.m. basis used in the expansion remain valid, the evolution was terminated in the calculation when the expected value of the energy,

$$\langle E(t)\rangle = \langle \Psi_{\text{tot}}^{\text{system}}(t)|E_{\text{kin}} + E_{\text{pot}}|\Psi_{\text{tot}}^{\text{system}}(t)\rangle, \tag{4.16}$$

was greater than some cutoff close to the trap depth. In practice, the evolution was performed by the split operator FFT method [20] in sufficiently small time steps δt chosen so that the change in $\|\Psi_{\text{tot}}^{\text{system}}(t)\rangle\|^2$ from t to $t+\delta t$ was negligible and the results became independent of δt.

The initial state (written as a spinor in the bare basis),

$$\langle \mathbf{r}, t=0|\Psi_{\text{tot}}^{\text{system}}\rangle = \frac{u_1(\rho,z)}{\sqrt{\rho}} e^{-im_0\phi} \otimes |D_0\rangle = \mathcal{T}^T(\mathbf{r}) \begin{pmatrix} \dfrac{u_1(\rho,z)}{\sqrt{\rho}} e^{-im_0\phi} \\ 0 \\ 0 \end{pmatrix}, \tag{4.17}$$

was used. According to Eq. (4.12) and as a consequence of the neglect of spontaneous emission, there will be no dynamical change to the ϕ part of the wave function, so that the distribution over $\{m\}$ factors out. In Eq. (4.17) an initial c.m. wave function with a well-defined $\Sigma_m c_{\lambda m} \to c_{\lambda m_0}$ is considered for simplicity; this point is discussed further in Sec. VI A. For now, it is sufficient to observe that $\langle E_c(t)\rangle$ is constant in time independent of this choice as long as the ϕ dependence is not entangled initially with the rest of the state. The ground state of the dressed basis was chosen as the initial internal state because it is the one which is affected by the full trapping potential. The calculations were run with a time step $\delta t = 10^{-7}$ s, which is a time scale much shorter than any of the dynamical rates, ensuring that the change in the c.m. wave function due to error in using the split operator FFT method is small, as discussed above. The c.m. energy $E_{\text{c.m.}}$ was calculated every 50 steps, or 5 μs, and checked until it reached -0.2 μK, which is $\sim \frac{1}{10}$ the well depth. At this point the calculation was stopped because beyond this it was assumed the atom could have significant contributions from the continuum. The states $\lambda = 1, \ldots, 5$ were used as the initial c.m. state and the results for the c.m. energy as a function of time for $\lambda = 1$, 2, and 4 are shown in Figs. 10, 11, and 12.

It is interesting to note that the $\lambda = 1$ state in Fig. 10 begins to get heated more rapidly than the states with

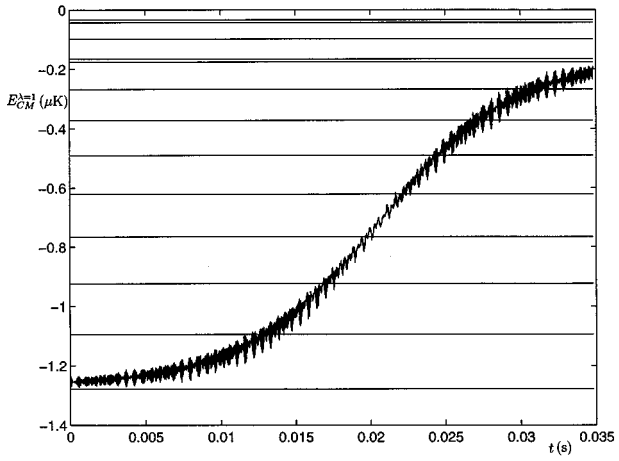

FIG. 10. The heating of the $\lambda(t=0)\equiv\lambda_0=1$ c.m. bound state for an atom initially in the ground dressed state $|D_0\rangle$. Initially, this state heats very quickly compared to the $\lambda_0=2,4$ states shown in Figs. 11 and 12. However, extrapolating suggests that it would take $\tau_{\text{heat}}(\lambda_0=1)\sim$ 40 ms for complete heating. In Sec. IV C the significance of the different rates evidenced in Figs. 10–12 is discussed and is further analyzed in Fig. 13. The time steps of the calculation on the time axis are $\Delta t=50\delta t=5$ μs.

$\lambda>1$, which tend to be increasingly stable with increasing λ until the onset of rapid heating. Heating times can be estimated by extrapolating the graphs to $E_{\text{c.m.}}\rightarrow 0$. Although this is a crude approximation, Figs. 10–12 all show a large energy decay rate $\Delta E_{\text{c.m.}}/\Delta t$ for $t\geqslant 20$ ms. These results will be discussed more quantitatively after first trying to make a semiclassical estimate of the heating rate.

C. Semiclassical analysis of momentum diffusion and comparison with quantum calculations

It is possible to estimate the rate of heating semiclassically using the concept of the momentum diffusion coefficient D. This coefficient can be calculated as follows [21]:

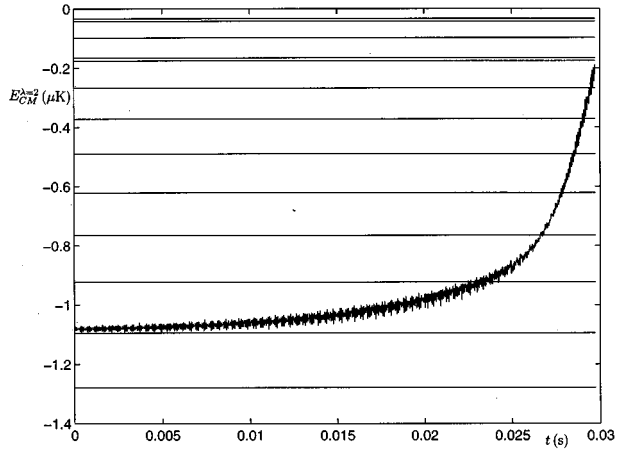

FIG. 11. The heating of the $\lambda_0=2$ c.m. bound state. This state stays close to the original energy of $E_{\text{c.m.}}(\lambda_0=2)$ for longer than in the case for $\lambda_0=1$ in Fig. 10. Complete heating here takes very close to $\tau_{\text{heat}}(\lambda_0=2)\sim 30$ ms.

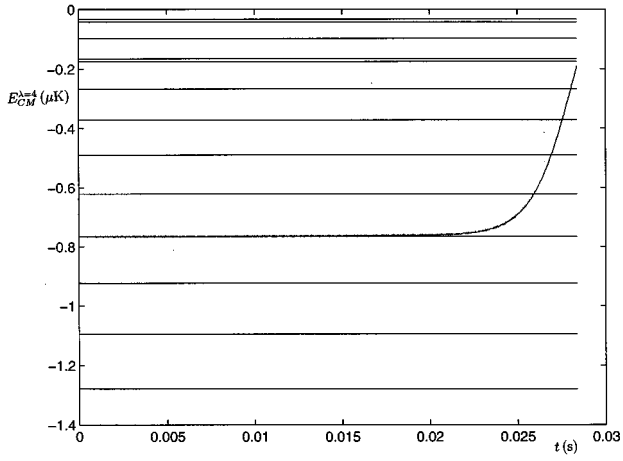

FIG. 12. The heating of the $\lambda_0=4$ c.m. bound state. The energy is very close to the original energy $E_{\text{c.m.}}(\lambda_0=4)$ throughout the atomic evolution before a very fast heating rate for $t>25$ ms.

$$
\begin{aligned}
D=&\hbar^2 k_{\text{laser}}^2\frac{\Gamma}{4}\frac{s}{1+s}+\hbar^2\boldsymbol{\beta}^2\frac{\Gamma}{4}\frac{s}{(1+s)^3}\\
&\times\left\{1+\frac{12\delta^2-\Gamma^2}{4\delta^2+\Gamma^2}s+s^2\right\}+\hbar^2\boldsymbol{\alpha}^2\frac{\Gamma}{4}\frac{s}{(1+s)^3}\\
&\times\left\{\begin{array}{l}1+\dfrac{-4\delta^2+3\Gamma^2}{4\delta^2+\Gamma^2}s\\ +3s^2+\dfrac{4\delta^2+\Gamma^2}{\Gamma^2}s^3\end{array}\right\}-\hbar^2\boldsymbol{\alpha}\cdot\boldsymbol{\beta}\delta\frac{s^2}{(1+s)^3}\\
&\times\left\{\frac{4\Gamma^2}{4\delta^2+\Gamma^2}+s\right\}. \qquad (4.18)
\end{aligned}
$$

In this expression, $\boldsymbol{\alpha}$ is the logarithmic gradient of the amplitude of the Rabi frequency Ω, $\boldsymbol{\beta}$ is the gradient of the phase of the Rabi frequency, and k_{laser} is the magnitude of the laser wave vector. This expression is valid only for a two-level atom. However, to the extent that coherences between the upper levels can be ignored, and due to the fact that the spontaneous rates for the two levels are very different, we will apply it to our three-level atom. Now, for the atom gallery as a FORT, $\delta\gg\Gamma$ and $s=\Omega^2/2\delta^2\ll 1$. Also, looking at the expressions for the electric field outside of the sphere [Eq. (2.1) with j_L replaced by the outgoing spherical Hankel function $h_L^{(1)}$ and k_{PL}^{TM} replaced by k_{PL}^{TM}/n], the quantities $\boldsymbol{\alpha}$ and $\boldsymbol{\beta}$ can easily be estimated from $\Omega=\tilde{\Omega}e^{i\Phi}$:

$$
\boldsymbol{\alpha}=\frac{\nabla\tilde{\Omega}}{\tilde{\Omega}}\sim\frac{\nabla(\Omega_0 e^{-i(k_{PL}^{\text{TM}}/n)r})}{\Omega_0 e^{-i(k_{PL}^{\text{TM}}/n)r}}=-i\frac{k_{PL}^{\text{TM}}}{n}\hat{\mathbf{e}}_r, \qquad (4.19)
$$

and since the WGMs are traveling waves,

$$
\boldsymbol{\beta}=\nabla\Phi=\frac{1}{\rho}\frac{\partial}{\partial\phi}(iM\phi)\hat{\mathbf{e}}_\phi\sim i\frac{M}{a}\hat{\mathbf{e}}_\phi. \qquad (4.20)
$$

D is then rewritten as

$$D=\hbar\left(\frac{k_{PL}^{\mathrm{TM}}}{n}\right)^2\frac{\Gamma}{4}s+\hbar^2\frac{M^2}{a^2}\frac{\Gamma}{4}s+\hbar^2\left(\frac{k_{PL}^{\mathrm{TM}}}{n}\right)^2\frac{\Gamma}{4}s\left\{1+\frac{4\delta^2}{\Gamma^2}s^3\right\}. \tag{4.21}$$

However, for both of the atom gallery WGMs relevant to the FORT, $M\sim L\sim k_{PL}^{\mathrm{TM}}a$, hence

$$D\sim\hbar^2\left(\frac{k_{PL}^{\mathrm{TM}}}{n}\right)^2\frac{\Gamma}{4}s\left\{2+n^2+\frac{4\delta^2}{\Gamma^2}s^3\right\}. \tag{4.22}$$

The free space spontaneous emission parameters satisfy $\Gamma_2\ll\Gamma_1$. (This is true also of the modified rates calculated in Sec. V B). The fact that Γ_1 should be the important rate can be seen from the Stark shifts in Eq. (4.10). The middle dressed state $|D_1\rangle$ associated with Γ_1 is affected by the most repulsive potential. In order to make absolute comparison with the dynamics in Sec. IV B which did not include spontaneous emission (which should be a reasonable approximation since $\tau_{\mathrm{heating}}\sim\Delta t_{\mathrm{emission}}$ as previously discussed), the term due to recoil heating is ignored. Finally, the term $(4\delta^2/\Gamma^2)s^3$ is down many orders of magnitude for all fields and states involved. Thus

$$D\sim\hbar^2\left(\frac{k_{P_1L_1}^{\mathrm{TM}}}{n}\right)^2\frac{\Gamma_1}{4}s_1(1+n^2). \tag{4.23}$$

As a diffusion coefficient, D can also be written

$$D=\frac{1}{2}\frac{d}{dt}\langle[\mathbf{p}(t)-\langle\mathbf{p}(t)\rangle]^2\rangle=\frac{1}{2}\frac{d}{dt}(\sigma_{\mathbf{p}}^2)\sim\frac{1}{2}\frac{\Delta(\mathbf{p}^2)}{\Delta t} \tag{4.24}$$

for c.m. momentum $\mathbf{p}$. Therefore

$$\frac{\Delta E_{\mathrm{c.m.}}}{\Delta t}\sim\frac{D}{m_c}\sim\frac{\hbar^2(k_{P_1L_1}^{\mathrm{TM}}/n)^2\Gamma_1 s_1(1+n^2)}{4m_c}. \tag{4.25}$$

Using $s_1=2\times10^{-6}$, $k_{P_1L_1}^{\mathrm{TM}}=6.9736\times10^6\ \mathrm{m}^{-1}$, $\Gamma_1/2\pi=1.15\times5.093$ MHz (the factor 1.15 to be explained in Sec. V B) gives $\Delta E_{\mathrm{c.m.}}/\Delta t\sim4\ \mu$K/s. From Figs. 10–12, this rate can be identified with the *initial* slopes in the heating curves which vary from $\sim3\ \mu$K/s for the $\lambda=1$ c.m. state to $\sim0.5\ \mu$K/s for the $\lambda=5$ c.m. state. Even though at a first glance the semiclassical expression in Eq. (4.25) is independent of c.m. state, the c.m. state dependence of D can be recovered by realizing that the expected value $\langle s_1(\mathbf{r})\rangle_\lambda$ should be taken *across the wave packet* of the state λ. Hence the semiclassical analysis seems to give a good quantitative understanding of the initial dynamics.

However, in all of the heating curves, a second heating rate dominates after $t\sim10$–20 ms. For example, for the $\lambda=1$ state a second rate of $\Delta E_{\mathrm{c.m.}}/\Delta t\sim60\ \mu$K/s starts at $t\sim15$ ms. The best way to understand this anomalous quantum heating is to look at the evolution of the coefficients $|c_{\lambda m_0}(t)|^2$, $|b_{\lambda' m_0}(t)|^2$, and $|d_{\lambda'' m_0}(t)|^2$ in Eq. (4.11). Both $|b_{\lambda' m_0}(t)|^2$ and $|d_{\lambda'' m_0}(t)|^2$ remain very small for all λ and for all time because the excited states never become appreciably populated, but in Fig. 13, $|c_{\lambda m_0}(t)|^2$ is plotted for the heating curve corresponding to the $\lambda=1$ c.m. state in Fig. 10. It is clear that the states $\lambda=8,9,12$ cause the very fast heating rate as their probabilities increase very quickly for $t\geqslant15$ ms. These states seem to be most unstable whereas all of the other states are relatively quiet. This heating cannot be understood from a purely semiclassical analysis. It would be interesting to redo the calculation for the 95 μK well to understand whether the small basis size of 13 c.m. states contributes to the quantum heating. Unfortunately, this was deemed too computationally intensive for the initial investigations.

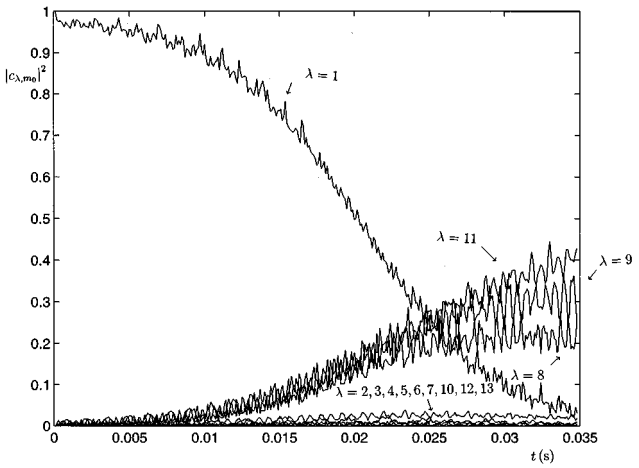

FIG. 13. The evolution of the coefficients of the bound states λ during the course of the heating of the initial bound state $\lambda_0=1$ shown in Fig. 10. The states $\lambda=7,8,9$ cause the rapid change in heating rate for $t\geqslant10$ ms, which cannot be predicted from semiclassical theory.

D. The quantum Monte Carlo wave function (QMCWF) approach

Finally, the possible use of the QMCWF approach [22] is discussed. In this approach, it would be necessary to add a non-Hermitian term (in the bare basis)

$$H_\Gamma=i\frac{1}{2}\begin{pmatrix}0&0&0\\0&\Gamma_1&0\\0&0&\Gamma_2\end{pmatrix} \tag{4.26}$$

to the Hamiltonian H in Eq. (4.13) to account for spontaneous decay processes. One would then generate a random number and monitor the norm of the wave function to decide if the system would undergo a spontaneous decay. Quantum jumps and state vector renormalizations are applied depending on the outcome. This method was applied to our system and, as motivated in qualitative terms above, it was found that the role of spontaneous emission was negligible and that the quantum evolution was unaffected. However, it must be emphasized that the jump operators associated with spontaneous emission in this system are very interesting objects because they depend intimately on the spherical symmetry of the atom gallery. This issue is discussed further in Sec. V C after first putting the whole question of spontaneous emission in a broader context.

V. RADIATIVE PROCESSES IN QUANTIZED ATOM-MICROSPHERE SYSTEMS

There are two important regimes in cavity QED in which the idea of spontaneous emission is discussed [23–25]. The first corresponds to a *perturbative regime* in which spontaneous emission into a complete set of reservoir modes acts to damp the atomic excited state at a rate Γ_0 which is much faster than the internal atomic dynamical rate Ω, also known as the Rabi frequency. The presence of a cavity can drastically affect the structure of the reservoir modes, causing an alteration to the spontaneous decay rate $\Gamma_0 \rightarrow \Gamma_{\text{cavity}}$. One must also make the further distinction between the situation in which no single reservoir mode is resonant with the atomic transition and the case where one of the modes moves close to atomic resonance. When the resonant mode has a high quality factor and Ω is simultaneously large, internal atomic dynamics can become dominant over both the cavity decay rate $\kappa = \omega_{\text{optical}}/2Q$ and the spontaneous rate Γ_{cavity} into all modes other than the privileged cavity mode. Here, we move into a *nonperturbative, strongly coupled* regime.

The quantization of the c.m. in the atom gallery is expected to modify somewhat the usual results in these two regimes. The FORT nature of the trap keeps the atom primarily in its internal ground state, so it might seem hopeless to try to understand the effect of the atom gallery c.m. wave functions on excited state decay. However, we can take advantage of the tremendous separation of time scales. In Sec. IV C, it was found that the wave packet decoherence time, $\tau_{\text{heating}} \sim 10$ ms, is much larger than the ~ 100 ns time scale for spontaneous decay. In what follows, then, the atomic c.m. is considered to be in a state λ but no longer in the presence of the FORT trapping fields so that it is free to decay from its internal excited state. Several authors have considered the effect of the quantization of the c.m. on spontaneous emission in more general terms [26,27].

A. Radiation field description

To understand the role of the reservoir in spontaneous emission, it is necessary to have a quantum description of the radiation field. The quantization procedure for the radiation field is that one must provide a *complete modal expansion* for this field respecting any boundary conditions [14]. This is done by solving the classical electromagnetics problem for the field in the given geometry. Any electromagnetic field *external* to the microsphere at fixed frequency $\omega = ck/n$, where n is the index of refraction of the sphere and k is the magnitude of the wave vector *inside* the sphere, can be expanded as [11]

$$\mathbf{E}_{\text{rad}}(\mathbf{r}) = \sum_{L,M} \left\{ \alpha_{\text{TM}}(L,M) \frac{n}{k} \boldsymbol{\nabla} \times \left[h_L^{(1)}\left(\frac{k_{PL}^{\text{TM}}}{n} r \right) \mathbf{Y}_{LLM}(\theta,\phi) \right] + \alpha_{\text{TE}}(L,M) h_L^{(1)}\left(\frac{k_{PL}^{\text{TM}}}{n} r \right) \mathbf{Y}_{LLM}(\theta,\phi) \right\}, \tag{5.1}$$

where the $\mathbf{Y}_{LLM}(\theta,\phi)$ are vector spherical harmonics. One then chooses the $\alpha_{\text{TE}}(L,M)$ and $\alpha_{\text{TM}}(L,M)$ to satisfy the boundary conditions. In the course of doing so for the microsphere case, *for any initial conditions* [28], one finds resonances in $\alpha_E(L,M)$ and $\alpha_M(L,M)$ at the microsphere modes k_{PL}^{TE} and k_{PL}^{TM}. The quantized field as a Schrödinger operator is then

$$\mathbf{E}_{\text{rad}}(\mathbf{r}) = \sum_{s,\mathbf{P}} \mathcal{N}_{\mathbf{P}}^{s} (a_{s,\mathbf{P}}\, \psi_{s,\mathbf{P}} + \text{H.c.}). \tag{5.2}$$

Only valid microsphere modes need now be considered. These modes are denoted $(s,\mathbf{P})$, where s labels the polarization (TE or TM), $\mathbf{P}=(P,L,M)$, $a_{s,\mathbf{P}}$ is a mode annihilation operator, and

$$\boldsymbol{\psi}_{\text{TM},\mathbf{P}} = \begin{cases} \psi_{\text{TM},\mathbf{P}}^{0} \dfrac{1}{k_{PL}^{\text{TM}}} \boldsymbol{\nabla} \times [j_L(k_{PL}^{\text{TM}} r) \mathbf{Y}_{LLM}(\theta,\phi)] \\ \psi_{\text{TM},\mathbf{P}}^{0} \dfrac{n}{k_{PL}^{\text{TM}}} \boldsymbol{\nabla} \times \left[h_L^{(1)}\left(\dfrac{k_{PL}^{\text{TM}}}{n} r \right) \mathbf{Y}_{LLM}(\theta,\phi) \right] \end{cases}$$

$$\boldsymbol{\psi}_{\text{TE},\mathbf{P}} = \begin{cases} \psi_{\text{TE},\mathbf{P}}^{0} j_L(k_{PL}^{\text{TE}} r) \mathbf{Y}_{LLM}(\theta,\phi) \\ \psi_{\text{TE},\mathbf{P}}^{0} h_L^{(1)}\left(\dfrac{k_{PL}^{\text{TE}}}{n} r \right) \mathbf{Y}_{LLM}(\theta,\phi), \end{cases} \tag{5.3}$$

with j_L $(h_L^{(1)})$ for $r <$ $(>) a$ and $\psi_{s,\mathbf{P}}^{0} = 1/\max(|\boldsymbol{\psi}_{s,\mathbf{P}}|)$. Note that the expressions for the microsphere modes in Eq. (2.1) are equivalent to the $r<a$ part of $\boldsymbol{\psi}_{\text{TM},\mathbf{P}}$ up to a normalization factor of $\sqrt{L(L+1)}$. This arises from the definition of $\mathbf{Y}_{LLM}(\theta,\phi) = [1/\sqrt{L(L+1)}]\mathbf{L} Y_{LM}(\theta,\phi)$. The factors $\mathcal{N}_{\mathbf{P}}^{s}$ are the normalization factors for the field modes. The field is normalized by taking the vacuum expectation value of the equation

$$U_{\text{field}} = \int_{V_Q} \left(\frac{1}{2} \varepsilon(\mathbf{r}) \mathbf{E}_{\text{rad}}(\mathbf{r}) \cdot \mathbf{E}_{\text{rad}}(\mathbf{r}) + \frac{1}{2} \mu(\mathbf{r}) \mathbf{B}_{\text{rad}}(\mathbf{r}) \cdot \mathbf{B}_{\text{rad}}(\mathbf{r}) \right) dV, \tag{5.4}$$

to get

$$U_{\text{field}} = \sum_{s,\mathbf{P}} \left(a_{s,\mathbf{P}}^{\dagger} a_{s,\mathbf{P}} + \frac{1}{2} \right) \hbar \omega_{PL}^{s}. \tag{5.5}$$

Thus

$$\mathcal{N}_{\mathbf{P}}^{s} = \sqrt{\frac{\hbar c k_{PL}^{s}}{2 n V_{s,\mathbf{P}}}}, \tag{5.6}$$

where

$$V_{s,\mathbf{P}} = \int_{V_Q} \varepsilon(\mathbf{r}) \boldsymbol{\psi}_{s,\mathbf{P}}^{2}(\mathbf{r}) dV \tag{5.7}$$

is defined as the effective mode volume for a quantization volume V_Q with

$$\varepsilon(\mathbf{r}) = \begin{cases} n^2, & r<a \\ 1, & r>a. \end{cases} \tag{5.8}$$

This definition for $V_{s,\mathbf{P}}$ can be compared with an expression for $V_{s,\mathbf{P}}$ used by Braginsky *et al.* [10] in the context of optical nonlinearity issues of fused silica microspheres,

$$V^{(1)}_{s,\mathbf{P}} \sim \frac{\left(\int_{V_Q} \boldsymbol{\psi}^2_{s,\mathbf{P}}(\mathbf{r}) dV \right)^2}{\int_{V_Q} [\boldsymbol{\psi}^2_{s,\mathbf{P}}(\mathbf{r})]^2 dV}, \tag{5.9}$$

which for the mode $(s,\mathbf{P})=(\mathrm{TM},P,L,M)$ gives

$$V^{(1)}_{s,\mathbf{P}} \approx 3.4\pi^{3/2} \left(\frac{1}{k^{\mathrm{TM}}_{PL}} \right)^3 L^{11/6} \sqrt{L-M+1}. \tag{5.10}$$

The definitions in Eqs. (5.9) and (5.7) give slightly different mode volumes as is discussed in physical terms in Ref. [29]. For example, for the mode $(\mathrm{TM},P,L,M)=(\mathrm{TM},1,492,488)$ Eq. (5.10) predicts $V^{(1)}_{s,\mathbf{P}}=3.52\times10^{-15}\ \mathrm{m}^3$ and calculations using Eq. (5.7) give $V_{s,\mathbf{P}}=6.56\times10^{-15}\ \mathrm{m}^3$ and for the mode $(\mathrm{TM},P,L,M)=(\mathrm{TM},1,996,996)$ Eq. (5.10) predicts $V^{(1)}_{s,\mathbf{P}}=0.72\times10^{-15}\ \mathrm{m}^3$ and calculations with Eq. (5.7) give $V_{s,\mathbf{P}}=1.29\times10^{-15}\ \mathrm{m}^3$. These both differ by the same factor of ~ 1.8.

B. Spontaneous emission in the perturbative regime with nonresonant WGMs

We consider first the situation of an initial atom gallery c.m. state λ which decays from the excited internal state. A photon is emitted by the atom into one mode of a set of radiation field modes, none of which is resonant with the atom so that a perturbative approach is valid. The case of an atom with a radial dipole $\mathbf{d}=d\hat{\mathbf{e}}_r$ which is localized around $(r,\theta,\phi)\sim(r_0,\pi/2,0)$ is considered. Using the fact that $\hat{\mathbf{e}}_r\cdot\mathbf{Y}_{LLM}(\theta,\phi)=0$, only the TM modes survive in the expansion in Eq. (5.1). In Eq. (5.1) applied to the problem at hand, the term $\alpha_{\mathrm{TM}}(L,M)$ is given by $\alpha_{\mathrm{TM}}(L,M)=\tilde{a}_{\mathrm{TM}}(L,M)+b_L a_{\mathrm{TM}}(L,M)$ where

$$a_{\mathrm{TM}}(L,M)=\frac{4\pi i}{n}k^2 \left\langle \mathbf{d}\cdot\boldsymbol{\nabla}\times\left[h^{(1)}_L\left(\frac{k}{n}r\right)\mathbf{Y}_{LLM}(\theta,\phi)\right]\right\rangle_\lambda \tag{5.11}$$

and

$$b_L=\frac{j_L(\rho)[n\rho j_L(n\rho)]'-n^2 j_L(n\rho)[\rho j_L(\rho)]'}{n^2 j_L(n\rho)[\rho h^{(1)}_L(\rho)]'-h^{(1)}_L(\rho)[n\rho j_L(n\rho)]'}. \tag{5.12}$$

Here, $\rho=(k^{\mathrm{TM}}_{PL}/n)a=(k/n)a$, a is the sphere radius, and $\tilde{a}_{\mathrm{TM}}=a_{\mathrm{TM}}(h^{(1)}_L\to j_L)$. The expectation value $\langle\rangle_\lambda$ in Eq. (5.11) is taken over the c.m. wave function λ because the exact location of the dipole is not known when the c.m. is quantized. The spontaneous rate is calculated by [24]

$$\begin{aligned}\frac{\Gamma_1(\lambda)}{\Gamma_1^{\mathrm{free}}}-1 &= \frac{3}{2}\left\langle \mathrm{Im}\left(\frac{\mathbf{d}\cdot\mathbf{E}^{\mathrm{sc}}(\mathbf{r})}{d^2k^3}\right)\right\rangle_\lambda \\ &= i\frac{6\pi}{d^2k^2}\mathrm{Re}\sum_{L,M}\left(b_L\left\langle\left\{\mathbf{d}\cdot\boldsymbol{\nabla}\times\left[h^{(1)}_L\left(\frac{k}{n}r\right)\mathbf{Y}^*_{LLM}(\theta,\phi)\right]\right\}\right.\right. \\ &\quad \left.\left.\times\left\{\mathbf{d}\cdot\boldsymbol{\nabla}\times\left[h^{(1)}_L\left(\frac{k}{n}r\right)\mathbf{Y}_{LLM}(\theta,\phi)\right]\right\}\right\rangle_\lambda\right),\end{aligned} \tag{5.13}$$

where $\mathbf{E}^{\mathrm{sc}}(\mathbf{r})$ is the operator corresponding to the scattered portion of the field only for which $\tilde{a}_{\mathrm{TM}}$ can be ignored and the 1 subscript refers to the $|1\rangle\to|0\rangle$ internal atomic transition. Using

$$\sum_{M=-L}^{L}\left[Y_{LM}\left(\frac{\pi}{2},0\right)\right]^2=\frac{2L+1}{4\pi}, \tag{5.14}$$

Eq. (5.13) becomes

$$\begin{aligned}\frac{\Gamma_1(\lambda)}{\Gamma_1^{\mathrm{free}}}-1 &= \frac{3}{2}\mathrm{Re}\left[\sum_{LM}P_{LM}(L,M)\right] \\ &= 6\pi\mathrm{Re}\left\{\sum_{L=1}^{\infty}L(L+1)b_L\left\langle\left(\frac{h_L(x)}{x}\right)^2\right\rangle_\lambda\right. \\ &\quad \left.\times\sum_{M=-L}^{L}\left[Y_{LM}\left(\frac{\pi}{2},0\right)\right]^2\right\} \\ &= \frac{3}{2}\mathrm{Re}\left[\sum_{L=1}^{\infty}L(L+1)(2L+1)b_L\left\langle\left(\frac{h_L(x)}{x}\right)^2\right\rangle_\lambda\right].\end{aligned} \tag{5.15}$$

Apart from the $\langle\rangle_\lambda$, this is the same expression as in Refs. [7,8] where these previous calculations have assumed the atom to be a radial dipole located at $(r_0,0,0)$ as opposed to $(r_0,\pi/2,0)$ here.

The evaluation of Eq. (5.15) was carried out for the parameters $a=50.04\ \mu$m and $\lambda_{\mathrm{optical}}=894.595$ nm that have been considered up until now. The numerical result is that there is an enhancement in the spontaneous emission by a factor of 1.15 for the $\lambda=1$ c.m. state. This result is dependent on the c.m. state, but not significantly; it changes by less than 5% from $\lambda=1$ to $\lambda=13$. This is clear when compared to the classical atomic position dependence of $\Gamma_1(\mathbf{r})/\Gamma_1^{\mathrm{free}}$ in Ref. [7]: $\Gamma_1(\mathbf{r})/\Gamma_1^{\mathrm{free}}$ changes over a scale of $\delta r/a\sim10\%$ whereas the c.m. wave function is localized to $\delta r/a\sim0.1\%$ for $\lambda=1$ up to only $\delta r/a\sim1\%$ for $\lambda=13$. However, the numerical factor $\Gamma_1(\lambda)/\Gamma_1^{\mathrm{free}}=1.15$ is itself extremely sensitive to the geometrical factors such as sphere radius a and atomic decay wavelength $\lambda_{\mathrm{optical}}$. The physical reason is simple: the actual value of $\Gamma_1(\lambda)$ is highly dependent on the precise location of the atomic resonance relative to the set of radiation modes and small changes to geometrical factors can unpredictably shift a mode onto resonance. This has

been discussed very clearly by Kleppner in Ref. [30] in which the ideas of inhibited and enhanced spontaneous emission are attributed to a careful evaluation of the mode sum.

It is also important to note that level frequency shifts accompany the changes in the radiative widths and are in fact the origin of the van der Waals and Casimir-Polder components of the c.m. potential in Eq. (2.2). Similar mode sums as above occur in the evaluation of these shifts, except that the individual modes now contribute a dispersive line shape to the sum. It is not expected that these shifts are important in the atom gallery system because of the distance of the atomic c.m. wave functions from the sphere; however, Ref. [6] has pursued this very interesting issue for microspheres using a classical atomic c.m. description.

C. Spontaneous emission in the perturbative regime with a resonant WGM

In the following, we consider the case for which the atomic transition is brought onto resonance with a particular WGM. The absorption-limited quality factors for certain WGMs can be greater than 10^9 in the optical domain [31–33], and in order that the perturbative regime remain valid, we must consider the case where the internal atomic Rabi frequency Ω is still much less than $\kappa=\omega_{\text{optical}}/2Q$. According to the estimates in Ref. [2] for a 50 μm radius sphere, we require $Q\leqslant 10^8$. One could also consider reducing Ω with respect to κ by using a larger sphere. Section V D will lift this restriction when we discuss the nonperturbative regime.

For concreteness, the resonant quantum field mode is taken to be the mode $(s,\mathbf{P}_1)=(\text{TM},P_1,L_1,M_1)$, with a frequency $\omega^{\text{TM}}_{P_1L_1}=ck^{\text{TM}}_{P_1L_1}$ and with $(P_1,L_1)=(1,492)$. In order to calculate the spontaneous rate $\Gamma_1(\Psi_{\text{c.m.}})$, we pull out the privileged cavity mode from all of the mode sums and calculate $\Gamma_1^{\text{res}}(\Psi_{\text{c.m.}})$. The contribution from all of the nonresonant modes, $\Gamma_1^{\text{nonres}}(\Psi_{\text{c.m.}})$, can proceed exactly as in the preceding section [i.e., Eq. (5.15)]. The only tricky point is that the modes (TM,P_1,L_1,M') with $M'\in[-L_1,L_1]$ must simultaneously be pulled out because they are also resonant (for a perfect sphere) with the mode $(s,\mathbf{P}_1)$. Henceforth we consider only the resonant contribution in the mode sum in Eq. (5.2) and in fact we will show that $\Gamma_1(\Psi_{\text{c.m.}})=\Gamma_1^{\text{res}}(\Psi_{\text{c.m.}})+\Gamma_1^{\text{nonres}}(\Psi_{\text{c.m.}})\approx\Gamma_1^{\text{res}}(\Psi_{\text{c.m.}})$. Therefore with $r>a$ we need consider only

$$\mathbf{E}_{\text{rad}}(\mathbf{r})=\sum_M \mathcal{N}^{\text{TM}}_{\mathbf{P}_1}\left(a_{\text{TM},\mathbf{P}_1}\left\{ \frac{n}{k^{\text{TM}}_{P_1L_1}}\boldsymbol{\nabla} \times\left[h^{(1)}_{L_1}\left(\frac{k^{\text{TM}}_{P_1L_1}}{n}r \right)\mathbf{Y}_{L_1L_1M}(\theta,\phi)\right]\right\}+\text{H.c.}\right). \quad (5.16)$$

1. Effect on the c.m. wave function

The effect of a radiated photon on the c.m. wave function is first examined because this will be useful in the discussions of the nonperturbative regime in Sec. V D and of the quantum jump picture in Sec. V E.

Spontaneous decay at $t=t^-_{\text{jump}}$ from the atomic internal state $|1\rangle$ will move all of the population to the ground internal state $|0\rangle$ so that only the initial atomic wave function

$$\langle \mathbf{r},t^-_{\text{jump}}|\Psi^{\text{system}}_{\text{tot}}\rangle\equiv\sum_{\lambda,m} c_{\lambda m}(t^-_{\text{jump}})\frac{u_\lambda(\rho,z)}{\sqrt{\rho}}e^{im\phi}\otimes|1\rangle \quad (5.17)$$

need be considered. The quantum jump expression for the total wave function can be written as

$$|\Psi^{\text{system}}_{\text{tot}}(t^-_{\text{jump}})\rangle\rightarrow\mathcal{C}\mathbf{d}_{01}\cdot\mathbf{E}_{\text{rad}}(\mathbf{r})|\Psi^{\text{system}}_{\text{tot}}(t^-_{\text{jump}})\rangle, \quad (5.18)$$

where $\mathbf{d}_{01}$ is the atomic dipole operator for the corresponding internal state $|1\rangle\rightarrow|0\rangle$ transition, the radiation field $\mathbf{E}_{\text{rad}}(\mathbf{r})$ is evaluated at the atomic c.m. position operator $\mathbf{r}$ [14], and $\mathcal{C}$ is some overall normalization. The calculation of the post-jump wave function becomes an evaluation of

$$\langle 0|\mathbf{d}_{01}|1\rangle\cdot\mathbf{E}_{\text{rad}}(\mathbf{r})|\Psi^{\text{atom}}_{\text{c.m.}}(t^-_{\text{jump}})\rangle\otimes|0\rangle. \quad (5.19)$$

Inserting a complete set of c.m. states [it is here that the completeness of the set of $\{u_\lambda(\rho,z)\}$ is relied upon] gives, up to normalization,

$$|\Psi^{\text{system}}_{\text{tot}}\rangle\rightarrow\langle 0|\mathbf{d}_{01}|1\rangle\cdot\left[\sum_{\text{c.m.}'}|\Psi^{\text{atom}}_{\text{c.m.}'}\rangle \times\langle\Psi^{\text{atom}}_{\text{c.m.}'}|\mathbf{E}_{\text{rad}}(\mathbf{r})|\Psi^{\text{atom}}_{\text{c.m.}}\rangle\otimes|0\rangle\right]. \quad (5.20)$$

The internal matrix element is calculated as follows:

$$\begin{aligned}\langle 0|\mathbf{d}_{01}|1\rangle&=\frac{e}{\sqrt{3}}\int f_0(R)Rf_1(R)R^2dR(\hat{\mathbf{e}}_0+\hat{\mathbf{e}}_1+\hat{\mathbf{e}}_{-1})\\&\equiv eX_R(\hat{\mathbf{e}}_0+\hat{\mathbf{e}}_1+\hat{\mathbf{e}}_{-1}),\end{aligned} \quad (5.21)$$

where a spherical basis has been used and internal radial functions $f_{0,1}(R)$ assumed. The final state can be written down by combining the internal state matrix element with the external state matrix element

$$\begin{aligned}\langle \mathbf{r},t^+_{\text{jump}}|\Psi^{\text{system}}_{\text{tot}}\rangle&=\langle \mathbf{r},t^+_{\text{jump}}|\Psi^{\text{atom}}_{\text{c.m.}}\rangle\otimes|\Psi^{\text{system}}_{\text{tot}}\rangle\\&=eX_R(\hat{\mathbf{e}}_0+\hat{\mathbf{e}}_1+\hat{\mathbf{e}}_{-1})\cdot\left\langle \mathbf{r}\left|\sum_{\text{c.m.}'}\right|\Psi^{\text{atom}}_{\text{c.m.}'}\right\rangle\\&\quad\times\langle\Psi^{\text{atom}}_{\text{c.m.}'}|\mathbf{E}_{\text{rad}}(\mathbf{r})|\Psi^{\text{atom}}_{\text{c.m.}}\rangle\otimes|0\rangle\\&=\sum_{\lambda',m'} c_{\lambda'm'}\frac{u_{\lambda'}(\rho,z)}{\sqrt{\rho}}e^{im'\phi}\otimes|0\rangle.\end{aligned} \quad (5.22)$$

Note that the $\{c_{\lambda'm'}\}$ should be renormalized to $\{\overline{c_{\lambda'm'}}\}$ as is

explained in Appendix A 3. As a reminder that in the quantum jump process only one photon is ever emitted, we write

$$c_{\lambda' m'} = c^{M}_{\lambda' m'}, \tag{5.23}$$

where the superscript M reminds us that there is now a photon in the radiated field in the mode $(\mathrm{TM}, P_1, L_1, M)$. The $c^{M}_{\lambda' m'}$ are defined by

$$c^{M}_{\lambda' m'} = eX_R(\hat{\mathbf{e}}_0 + \hat{\mathbf{e}}_1 + \hat{\mathbf{e}}_{-1}) \cdot \mathcal{N}^{\mathrm{TM}}_{\mathbf{P}_1} \times \sum_{\lambda, m} c_{\lambda m} \int d^3\mathbf{r}' \left(\frac{u_{\lambda'}(\rho', z')}{\sqrt{\rho'}} \times e^{-im'\phi'} \mathbf{G}_{\mathbf{P}_1}(\mathbf{r}') \frac{u_{\lambda}(\rho', z')}{\sqrt{\rho'}} e^{im\phi'} \right), \tag{5.24}$$

and

$$\mathbf{G}_{\mathbf{P}_1}(\mathbf{r}') = \sqrt{L_1(L_1+1)} \times \left(\left[\frac{n}{k_{P_1 L_1}} \left(\frac{d}{dr'} + \frac{L_1+1}{r'} \right) h^{(1)}_{L_1} \left(\frac{k_{P_1 L_1}}{n} r' \right) \right] \left\{ \begin{array}{c} \sqrt{\frac{(L_1+1)(L_1-M)(L_1+M)}{(2L_1+1)L_1(2L_1-1)}} Y_{L_1-1,M}(\theta', \phi') \hat{\mathbf{e}}_0 \\ + \sqrt{\frac{(L_1+1)(L_1+M)(L_1+M-1)}{(2L_1+1)2L_1(2L_1-1)}} Y_{L_1-1,M-1}(\theta', \phi') \hat{\mathbf{e}}_1 \\ + \sqrt{\frac{(L_1+1)(L_1-M)(L_1-M-1)}{(2L_1+1)2L_1(2L_1-1)}} Y_{L_1-1,M+1}(\theta', \phi') \hat{\mathbf{e}}_{-1} \end{array} \right\} + \left[\frac{n}{k_{P_1 L_1}} \left(\frac{d}{dr'} - \frac{L_1}{r'} \right) h^{(1)}_{L_1} \left(\frac{k_{P_1 L_1}}{n} r' \right) \right] \left\{ \begin{array}{c} - \sqrt{\frac{L_1(L_1-M+1)(L_1+M+1)}{(2L_1+1)(L_1+1)(2L_1+3)}} Y_{L_1+1,M}(\theta', \phi') \hat{\mathbf{e}}_0 \\ + \sqrt{\frac{L_1(L_1-M+1)(L_1-M+2)}{(2L_1+1)2(L_1+1)(2L_1+3)}} Y_{L_1+1,M-1}(\theta', \phi') \hat{\mathbf{e}}_1 \\ + \sqrt{\frac{L_1(L_1+M+1)(L_1+M+2)}{(2L_1+1)2(L_1+1)(2L_1+3)}} Y_{L_1+1,M+1}(\theta', \phi') \hat{\mathbf{e}}_{-1} \end{array} \right\} \right). \tag{5.25}$$

Using the fact that integration over ϕ' in Eq. (5.24) causes selection in the variable m', it can be seen that the atom can only get kicked rotationally into certain c.m. states $\{e^{im'\phi}\}$ which enforce conservation of angular momentum.

2. Cavity enhanced spontaneous emission parameter

Turning to the actual evaluation of the resonant contribution to $\Gamma_1(\Psi_{\mathrm{c.m.}})$, we can apply Fermi's golden rule in the perturbative regime to the decay of atom into the special set of resonant modes $\{(\mathrm{TM}, P_1, L_1, M')\}$ with $M' \in [-L_1, L_1]$,

$$\begin{aligned} \Gamma_1(\Psi_{\mathrm{c.m.}}) &= \frac{2\pi}{\hbar} \sum_{\mathrm{final}} \left| \langle \Psi^{\mathrm{system}}_{\mathrm{final}} | \mathbf{d}_{01} \cdot \mathbf{E}_{\mathrm{rad}}(\mathbf{r}) | \Psi^{\mathrm{atom}}_{\mathrm{c.m.}} \rangle \right|^2 \rho(E_F)\, \delta(E_F - E_I) \\ &= \frac{2\pi}{\hbar} \int \rho(E_F) dE_F \sum_{\mathrm{c.m.}'} \left| eX_R(\hat{\mathbf{e}}_0 + \hat{\mathbf{e}}_1 + \hat{\mathbf{e}}_{-1}) \cdot \langle \Psi^{\mathrm{atom}}_{\mathrm{c.m.}'} | \mathbf{E}_{\mathrm{rad}}(\mathbf{r}) | \Psi^{\mathrm{atom}}_{\mathrm{c.m.}} \rangle \right|^2 \delta(E_F - E_I). \end{aligned} \tag{5.26}$$

We now just look at a single outcome: the photon is emitted into the final state $(\mathrm{TM}, P_1, L_1, M)$. In the end, we sum over all possible outcomes $M \in \{M' = [-L_1, L_1]\}$. Using completeness of the c.m. states, we can simplify the sum in the last line of Eq. (5.26),

$$\begin{aligned} F &\equiv \left| eX_R(\hat{\mathbf{e}}_0 + \hat{\mathbf{e}}_1 + \hat{\mathbf{e}}_{-1}) \cdot \sum_{\mathrm{c.m.}'} |\Psi^{\mathrm{atom}}_{\mathrm{c.m.}'}\rangle \langle \Psi^{\mathrm{atom}}_{\mathrm{c.m.}'} | \mathbf{E}_{\mathrm{rad}}(\mathbf{r}) | \Psi^{\mathrm{atom}}_{\mathrm{c.m.}} \rangle \right|^2 = \left| \sum_{\mathrm{c.m.}'} |\Psi^{\mathrm{atom}}_{\mathrm{c.m.}'}\rangle eX_R(\hat{\mathbf{e}}_0 + \hat{\mathbf{e}}_1 + \hat{\mathbf{e}}_{-1}) \cdot \langle \Psi^{\mathrm{atom}}_{\mathrm{c.m.}'} | \mathbf{E}_{\mathrm{rad}}(\mathbf{r}) | \Psi^{\mathrm{atom}}_{\mathrm{c.m.}} \rangle \right|^2 \\ &= \sum_{\mathrm{c.m.}'} \left| eX_R(\hat{\mathbf{e}}_0 + \hat{\mathbf{e}}_1 + \hat{\mathbf{e}}_{-1}) \cdot \langle \Psi^{\mathrm{atom}}_{\mathrm{c.m.}'} | \mathbf{E}_{\mathrm{rad}}(\mathbf{r}) | \Psi^{\mathrm{atom}}_{\mathrm{c.m.}} \rangle \right|^2. \end{aligned} \tag{5.27}$$

Comparing the second line of Eq. (5.27) with Eq. (5.22),

$$F=\left|\int d^3\mathbf{r}|\mathbf{r}\rangle\sum_{\lambda',m'} c^M_{\lambda'm'}\frac{u_{\lambda'}(\rho,z)}{\sqrt{\rho}}e^{im'\phi}\otimes|0\rangle\right|^2=\sum_{\lambda',m',\lambda'',m''}\left(c^M_{\lambda'm'}(c^M_{\lambda''m''})^*\int d^3\mathbf{r}\frac{u_{\lambda'}(\rho,z)u_{\lambda''}(\rho,z)}{\rho}e^{i(m'-m'')\phi}\right)$$

$$=\sum_{\lambda',m',\lambda'',m''}[c^M_{\lambda'm'}(c^M_{\lambda''m''})^*\delta_{\lambda',\lambda''}\delta_{m',m''}]=\sum_{\lambda',m'}|c^M_{\lambda'm'}|^2\equiv P_M(M). \tag{5.28}$$

The function $P_M(M)$ will be discussed in detail in Sec. V E.

The next important issue in calculating $\Gamma_1(\Psi_{\text{c.m.}})$ is the density of states term $\rho(E_F)$ for the resonant contribution. For a microsphere close to one of these resonances, it is not possible to turn a mode sum into an integral over many modes. However, it is possible to quantify the integral over a *particular* mode by considering the detailed mode structure. The best way to think about this is to consider only the resonant terms in the field of Eq. (5.1),

$$\mathbf{E}_{\text{rad}}\{\mathbf{r}\}=\sum_M\left\{b_L a_{\text{TM}}(L,M)\frac{n}{k}\boldsymbol{\nabla}\times\left[h_L^{(1)}\left(\frac{k^{\text{TM}}_{PL}}{n}r\right)\mathbf{Y}_{LLM}(\theta,\phi)\right]\right\}, \tag{5.29}$$

which have $b_L\to\infty$ because of the resonance condition (see Appendix A 1 a). For the particular resonant mode, we need to incorporate a small imaginary part. More correctly, $|b_L|^2$ contains the information about the resonance width and in particular Ref. [34] shows how $|b_L|^2$ is well represented by a Lorentzian line shape $g_{\mathcal{L}}(\omega)$ for the particular frequency of the emitted photon. Continuing to consider the mode $(s,\mathbf{P}_1)=(M,L_1,P_1)$, this leads to the form

$$\rho(\omega)=g_{\mathcal{L}}(\omega)=\frac{\Delta\omega^{\text{TM}}_{P_1L_1}/2\pi}{(\omega-\omega^{\text{TM}}_{P_1L_1})^2+(\Delta\omega^{\text{TM}}_{P_1L_1}/2)^2}, \tag{5.30}$$

where $\Delta\omega^{\text{TM}}_{\mathbf{P}_1L_1}$ is the resonance width. Returning to the evaluation of $\Gamma_1(\Psi_{\text{c.m.}})$ by summing over possible final states, we find

$$\Gamma_1(\Psi_{\text{c.m.}})=\frac{2\pi}{\hbar}\int\rho(\omega)d\omega\sum_{M'}P_M(M')\delta(E_F-E_I). \tag{5.31}$$

The factors $(\mathcal{N}^{\text{TM}}_{\mathbf{P}_1})^2=\hbar ck^{\text{TM}}_{P_1L_1}/2nV_{\text{TM},\mathbf{P}_1}$ and $e^2X_R^2$ are explicitly removed from $P_M(M')$ by defining

$$\frac{\hbar ck^{\text{TM}}_{P_1L_1}}{2nV_{\text{TM},\mathbf{P}_1}}e^2X_R^2\widetilde{P}_M(M')\equiv P_M(M'). \tag{5.32}$$

Hence

$$\Gamma_1(\Psi_{\text{c.m.}})=\frac{2\pi}{\hbar}\frac{\hbar\omega^{\text{TM}}_{P_1L_1}}{2}e^2X_R^2\sum_{M'}\frac{1}{V_{\text{TM},\mathbf{P}_1}}\widetilde{P}_M(M')\times\int\rho(\omega)d\omega\,\delta(\hbar\omega-\hbar\omega^{\text{TM}}_{P_1L_1}+\delta E_{\text{c.m.}})$$

$$=\frac{2\omega^{\text{TM}}_{P_1L_1}e^2X_R^2}{\hbar\Delta\omega^{\text{TM}}_{P_1L_1}}\sum_{M'}\frac{1}{V_{\text{TM},\mathbf{P}_1}}\widetilde{P}_M(M'), \tag{5.33}$$

where it is assumed that the c.m. energy shift $\delta E_{\text{c.m.}}\sim\hbar k^2/2m$ is much less than the resonance width (see Appendix A 1 b). Using the free space spontaneous emission parameter $\Gamma_1^{\text{free}}=(e^2X_R^2/3\pi\hbar)k^3$, noting that k pertains to the value outside the sphere, and relabeling $M'\to M$, the final result is

$$\frac{\Gamma_1(\Psi_{\text{c.m.}})}{\Gamma_1^{\text{free}}}=\frac{6\pi}{k^3}\left(\frac{\omega^{\text{TM}}_{P_1L_1}}{\Delta\omega^{\text{TM}}_{P_1L_1}}\right)\sum_M\frac{1}{V_{\text{TM},\mathbf{P}_1}}\widetilde{P}_M(M)=\frac{6\pi Q^{\text{TM}}_{P_1L_1}}{k^3}\sum_M\frac{1}{V_{\text{TM},\mathbf{P}_1}}\widetilde{P}_M(M), \tag{5.34}$$

where the resonance quality factor $Q^{\text{TM}}_{P_1L_1}\equiv(\omega^{\text{TM}}_{P_1L_1}/\Delta\omega^{\text{TM}}_{P_1L_1})$ has been identified.

It can be verified at a glance that this agrees with the known (e.g., [30]) resonant enhancement $\Gamma_{\text{cavity}}/\Gamma_0\sim Q\lambda^3_{\text{optical}}/V$ because the $V_{\text{TM},\mathbf{P}_1}$ are not very dependent on M and $\Sigma_M\widetilde{P}_M(M)$ is a scaling factor dependent on the overlap of the atomic c.m. state and the mode volume. The value $Q=10^8$ is used to calculate the ratio $\Gamma_1(\Psi_{\text{c.m.}})/\Gamma_1^{\text{free}}$ for the c.m. states $\lambda=1,\ldots,6$, with the results plotted in Fig. 14 for jumps of type J_1 (namely, $|1\rangle\to|0\rangle$). Note that enhance-

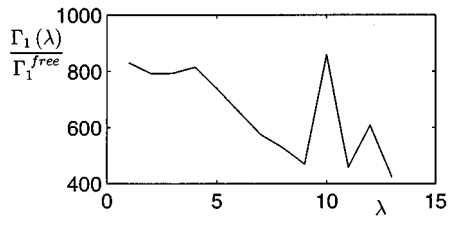

FIG. 14. The spontaneous emission rate $\Gamma_1(\lambda)$ normalized to the free space result Γ_1^{free} as calculated in Sec. V C 2. Note the dependence of the $\Gamma_1(\lambda)$ on the particular c.m. state due to the structure of the c.m. wave function. For example, the modes $\lambda=10,12$ corresponding to azimuthal excitation (see Fig. 8) are anomalously high because they keep the atomic c.m. probability closer to the dielectric interface.

ments over the free space rate by $\sim$ 800 are found for transition at 894.5 nm. By contrast, the enhancement for the $|2\rangle \rightarrow |0\rangle$ (or J_2 type) transition at 455.6 nm is ~ 5 with the difference in the two due to the factor $\lambda^3_{\text{optical}}$ and the difference in field amplitude for the two modes at the atomic position. This proves the resonant contribution dominates the sum of the off-resonant mode contributions. More significantly, for a given type of jump (J_1, J_2), the spontaneous rates are not wildly dependent on c.m. wave function λ as also found in the preceding section. However, the enhancement factors in the c.m. states $\lambda = 10,12$ (corresponding to $\hat{\mathbf{e}}_z$ excitations) are noticeably larger than their $\hat{\mathbf{e}}_\rho$ counterparts which is evidence for possible novel c.m. state effects on the dynamics; for example, a c.m. transition from an $\hat{\mathbf{e}}_\rho$ excitation state (e.g., $\lambda = 9$) to an $\hat{\mathbf{e}}_z$ excitation state (e.g., $\lambda = 10$) would change the internal atomic decay rate.

D. The nonperturbative regime

When the Q of the resonant mode becomes so high that a perturbative expansion is no longer formally valid, the coupled atom-cavity mode dynamics can be understood as an oscillatory exchange of quanta at the Rabi rate Ω. The perturbative calculation for the nonresonant modes in Sec. V B is still necessary to get the correct decay rate Γ_{cavity} into the reservoir, but the photons which couple into the resonant mode now have a long enough cavity lifetime $\sim \kappa^{-1}$ that they might be absorbed and reemitted into this mode several times before they are lost to the reservoir via Γ_{cavity}. The typical enhancement factor is called the single atom cooperativity $C_1 \sim g^2/\kappa\Gamma_{\text{cavity}}$ [35] (with $g = \Omega/2$ for a single photon in the cavity), but it can be shown to be equivalent to $\sim Q\lambda^3_{\text{optical}}/V$ as calculated perturbatively above for a dominant resonant mode. The major difference now is that the atom can also reabsorb the photon from the resonant cavity mode and a perturbative approach could never give a correct understanding of the coupled dynamics. The implication of this continuous coherent exchange for the c.m. wave function is a very interesting question. Qualitatively at least, the results of Sec. V C 1 indicate that each exchange conserves total angular momentum (more on this in Sec. V E below) and must lead to a diffusion of the $e^{im\phi}$ part of the wave function.

E. Interpretation of $P_M(M)$ in the quantum jump picture

1. Symmetry and the jump operators

A guiding light in this work has been the calculation of Marte *et al.* [36], in which an atom is placed in a potential representing quantized 1D molasses. In their case, the translational symmetry of the standing wave light field allows them to express not only the c.m. wave function in terms of a basis of Bloch functions but also to express simply the effect of the spontaneous emissions on this wave function. They quantize the radiation field as plane wave states inside a box appropriate to the boundary conditions. A photon emission then must cause atomic recoil according to $\langle z,t|\Psi^{\text{atom}}_{\text{c.m.}}\rangle \rightarrow e^{-i\mathbf{k}\cdot\hat{\mathbf{e}}_z}\langle z,t|\Psi^{\text{atom}}_{\text{c.m.}}\rangle$. This is just a translation of the Bloch vector with a strength determined by the probability distribution over angles for the emitted photon as contained in the dot product $\mathbf{k}\cdot\hat{\mathbf{e}}_z$ and this transformation, characterized by the jump operator $e^{-i\mathbf{k}\cdot\hat{\mathbf{e}}_z}$, summarizes the effect of the sponatneous decay quantum jump for the c.m. wave function. The decay rate Γ is just the free space result.

In order to gain an equivalent understanding of the atom gallery, its symmetry must be exploited. It is clear that the potential is ϕ independent and that any rotation of the system about the z axis by an angle of 2π causes no change to the system. As in the 1D molasses case, a spontaneous emission event breaks this symmetry, but the corresponding kick to the c.m. wave function should respect the symmetry of the c.m. basis. In the 1D molasses case, this is a translation in linear momentum but here it should correspond to a boost in angular momentum.

If one writes down the electromagnetic analog of the angular momentum operator $\mathbf{L}$,

$$\mathbf{L}_{\text{EM}} = \int_{V_Q} \mathbf{r} \times [\mathbf{E}_{\text{rad}}(\mathbf{r}) \times \mathbf{B}^*_{\text{rad}}(\mathbf{r})]\, dV, \tag{5.35}$$

and then proceeds to calculate the projection of this operator along the z axis, one finds [37]

$$L_{\text{EM},z} = \mathbf{L}_{\text{EM}} \cdot \hat{\mathbf{e}}_z = \sum_{s,\mathbf{P}} \hbar M \left(a^\dagger_{s,\mathbf{P}} a_{s,\mathbf{P}} + \frac{1}{2} \right), \tag{5.36}$$

which, when evaluated in a field state with a single photon in the mode $(s,\mathbf{P}_1)$ will give $\langle L_{\text{EM},z}\rangle = \hbar M$. In other words, it is not a linear momentum kick which is applied back on the c.m. wave function as in the case of 1D molasses, but it is an angular momentum kick and the overall process has had to conserve angular momentum.

In the nonresonant, perturbative regime it is sufficient to note from Eq. (5.15) that the function $P_{LM}(L,M)$, suitably normalized, forms a probability distribution for the photon to be emitted into the mode (L,M). This is the analogy to the distribution $p_{\mathbf{k}}(\mathbf{k})d\Omega_{\mathbf{k}} \sim |\hat{\mathbf{e}}_{\mathbf{d}} \times \hat{\mathbf{e}}_{\mathbf{k}}|^2 d\Omega_{\mathbf{k}}$ for a dipole in free space along $\hat{\mathbf{e}}_{\mathbf{d}}$ to emit a photon into the plane wave mode **k,** which is essential in understanding the form of the c.m. jump operator if one thinks of an emission event as a quantum jump.

In the resonant perturbative regime, the c.m. wave function changes due to a spontaneous emission into a dominant cavity mode. Equations (5.22)–(5.25) in fact specify the jump operators for a spontaneous emission into a dominant mode in the atom gallery by showing explicitly how the c.m. wave function is transformed. The jump operator cannot be simplified further because there are separate changes to both the $u_\lambda(\rho,z)$ and $e^{im\phi}$ part of the wave function. Again a situation arises where a function $P_M(M)$, defined in Eq. (5.28), acts as a probability distribution for a photon to be kicked into a radiation mode with orbital mode number M. In Fig. 15, the normalized version $P_M(M)$ of $P_M(M)$ is plotted for a jump of type J_1 for an atom in the state

$$|\psi_{\text{c.m.,ground}}\rangle \otimes |\psi_{\text{dressed,ground}}\rangle, \tag{5.37}$$

which is written out explicitly in Eq. (4.17). Note that this distribution is symmetric for $M \rightarrow -M$ and that the probability is very strongly peaked at $|M| \approx L_1$.

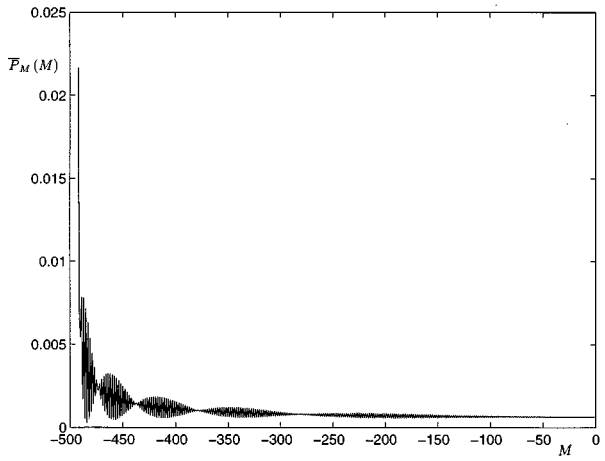

FIG. 15. The normalized probability distribution $\overline{P_M}(M)$ for a photon to be emitted with $M \in [-L_1, L_1]$ in a spontaneous emission event *in a resonant regime* from the internal atomic state $|1\rangle$ to the state $|0\rangle$. The initial c.m. state is taken to be $\lambda = 1$. Note that the distribution is symmetric about $M = 0$. This probability distribution is used to pick the $\hat{\mathbf{e}}_z$ component of the orbital angular momentum of a spontaneously emitted photon in the case of a jump of type J_1. It is the microsphere analogy to picking the $\hat{\mathbf{e}}_z$ component of the linear momentum of an emitted photon in free space according to a dipole distribution $p_{\mathbf{k}}(\mathbf{k})d\Omega_{\mathbf{k}} \sim |\hat{\mathbf{e}}_{\mathbf{d}} \times \hat{\mathbf{e}}_{\mathbf{k}}|^2 d\Omega_{\mathbf{k}}$ for a dipole along $\hat{\mathbf{e}}_{\mathbf{d}}$.

2. Significance of the jump process

The first observation is that *global* angular momentum conservation between internal states, external states, and the quantum radiation field has to be enforced. This is a practical example of something that has been discussed by van Enk [38] and others. The internal angular momentum appears due to the dot product of the spherical basis vectors with the quantum radiation field operator in Eq. (5.22). The phase $e^{iM\phi}$ of the radiation field in turn couples to the phase $e^{im\phi}$ of the c.m. wave function, causing a diffusion to an initially well-defined phase and the consequence of this on the dynamics will be discussed in the next section.

A second comment is that when using these jump operators in the quantum jump picture, it is implicitly assumed that our measuring device has the ability to distinguish the M value of the emitted photon. This may not be practical or even physically realizable. However, as Ref. [39] explains for the case of 1D molasses, the jump operators are not unique. This is true in general for any master equation. In the 1D molasses case, for example, one is able to do a unitary transformation on the jump operators from $B_\sigma(z)e^{-i\mathbf{k}\cdot\hat{\mathbf{e}}_z z}$ to $\int d\Omega_{\mathbf{k}} B_\sigma(z) e^{-ik\cos\theta(z-\nu\lambda/2)}$. This corresponds to a change in the measurement from the angular position of the emitted photon to c.m. wave function position localization by looking at the fluorescence through a lens. Such a transformation is known as a localizing quantum jump. One would hope that a similar transformation could be found here which would avoid relying upon the measurement of photon angular momentum. This is something to be investigated further.

Finally, and most importantly, the significance of the spherical geometry is evident. The angular momentum kick causes c.m. transitions and a change to $E_{\text{c.m.}}$, but the majority of the recoil energy must go into centrifugal energy E_c associated with the change in angular momentum *and this energy is largely decoupled from trap heating*. The sphere will thus tend to shield the atom from recoil heating in the transverse ($\hat{\mathbf{e}}_\rho$ and $\hat{\mathbf{e}}_z$) dimensions. This is not the case in other geometries: for example, the random direction for a linear momentum kick in 1D molasses is a limit to the cooling.

3. The limit of a large number of jumps

It is interesting to consider semiquantitatively the effect on the quantum dynamics if there were many spontaneous emission quantum jumps. Even though such a scenario cannot be compared with the actual dynamics calculated for our system in Sec. IV since there were very few jumps by design of the chosen parameters, this would become important either in the context of interaction of the c.m. wave packets with a quantum field, or simply for deeper wells. The number of jumps j scales as $j \sim \tau_{\text{heating}}/\Delta t_{\text{emission}}$ and the heating time τ_{heating} should scale as $\tau_{\text{heating}} \propto \Delta E_{\text{c.m.}}\, s\Gamma$. For the 95 μK potential, $E^{95\,\mu\text{K}}_{\text{c.m.}}(\lambda=1)/E^{2\,\mu\text{K}}_{\text{c.m.}}(\lambda=1) \sim 100$ and so $j^{95\,\mu\text{K}}/j^{2\,\mu\text{K}} \sim 100$ since the ratio is independent of $1/s\Gamma$. This would be noticeable in the number of orbits n_{orbit} that the atom could make around the sphere. The orbital period T_{orbit} scales as $T_{\text{orbit}} = \tau_{\text{heating}}/n_{\text{orbit}} = 2\pi a/v_\phi \sim 2\pi a^2 m_c/\hbar m_0$ where m_0 is the center of the distribution in $\{m\}$ for the c.m. wave function. Heating due to recoil effects, which was not present in previous calculations of τ_{heating} in Sec. IV C, can change n_{orbit} in the limit that there are a large number of jumps j.

For angular momentum conservation for the microsphere trap,

$$\mathbf{J}_{\text{atom}} \cdot \hat{\mathbf{e}}_z \rightarrow \mathbf{J}'_{\text{atom}} \cdot \hat{\mathbf{e}}_z + \mathbf{L}_{\text{EM}} \cdot \hat{\mathbf{e}}_z\,, \tag{5.38}$$

where $\mathbf{J}^{\text{tot}}_{\text{atom}} = \mathbf{L}^{\text{int}}_{\text{atom}} + \mathbf{L}^{\text{c.m.}}_{\text{atom}}$ and, as described explicitly above in Sec. V C 1,

$$m \rightarrow \left\{ \begin{array}{c} m+M-1 \\ m+M \\ m+M+1 \end{array} \right\}. \tag{5.39}$$

This transformation says that even if *all* of the quantum jumps are recorded, there will be a corresponding *spread* in the c.m. angular momentum. The reason for this is that there is an internal component, $\mathbf{L}^{\text{int}}_{\text{atom}}$ to the total angular momentum, $\mathbf{J}^{\text{tot}}_{\text{atom}}$ which cannot be ignored.

For an initial system wave function before the first jump at $t = t^-_{\text{jump}}$

$$\begin{aligned} \langle \mathbf{r}, t^-_{\text{jump}} | \Psi^{\text{system}}_{\text{tot}} \rangle &= \langle \mathbf{r}, t^-_{\text{jump}} | \Psi^{\text{atom}}_{\text{c.m.}} \rangle \otimes | \Psi^{\text{atom}}_{\text{int}} \rangle \\ &= e^{im_0\phi} \left(\begin{array}{c} \sum_\lambda c_\lambda(t^-_{\text{jump}}) \dfrac{u_\lambda(\rho,z)}{\sqrt{\rho}} \\ \sum_{\lambda'} b_{\lambda'}(t^-_{\text{jump}}) \dfrac{u_{\lambda'}(\rho,z)}{\sqrt{\rho}} \\ \sum_{\lambda''} d_{\lambda''}(t^-_{\text{jump}}) \dfrac{u_{\lambda''}(\rho,z)}{\sqrt{\rho}} \end{array} \right), \end{aligned} \tag{5.40}$$

the action on the ϕ part of the c.m. wave function by the jump operator at the first quantum jump from $|1\rangle\rightarrow|0\rangle$ is to take the initial m_0 in $e^{im_0\phi}$ and change it to

$$m_0\rightarrow\{m_0+M-1,m_0+M,m_0+M+1\}, \tag{5.41}$$

where M is a random variable corresponding to the final field state and is chosen from $P_M(M)$. If the normalized c.m. wave function is rewritten just after the jump,

$$\langle \mathbf{r},t^+_{\rm jump}|\Psi^{\rm system}_{\rm tot}\rangle=\begin{pmatrix}\sum_{\lambda,m}\overline{c_{\lambda m}}(t^+_{\rm jump})\dfrac{u_\lambda(\rho,z)}{\sqrt{\rho}}e^{im\phi}\\ 0\\ 0\end{pmatrix}, \tag{5.42}$$

the internal states will mix to produce a new wave function at a later time t' of the form

$$\langle \mathbf{r},t'|\Psi^{\rm system}_{\rm tot}\rangle=\begin{pmatrix}\sum_{\lambda,m}c_{\lambda m}(t')\dfrac{u_\lambda(\rho,z)}{\sqrt{\rho}}e^{im\phi}\\ \sum_{\lambda',m}b_{\lambda' m}(t')\dfrac{u_{\lambda'}(\rho,z)}{\sqrt{\rho}}e^{im\phi}\\ \sum_{\lambda'',m}d_{\lambda'' m}(t')\dfrac{u_{\lambda''}(\rho,z)}{\sqrt{\rho}}e^{im\phi}\end{pmatrix}. \tag{5.43}$$

It is evident that all three wave function spinor components contain exactly the same number of terms in m and that the entire wave function spreads out in m in exactly the same way. In fact, it is easy to see that after j spontaneous jumps there will be $N_m(j)=2j+1$ terms in Σ_m. After starting out in the state with total energy $E_{\rm tot}(t=0)=\hbar^2m_0^2/2m_ca^2$, the change in the energy after one jump of type M is given by

$$\delta E_{\rm tot}=\frac{\hbar^2}{2m_ca^2}\left[\sum_{\lambda,m}m^2|\overline{c_{\lambda m}}(t^+_{\rm jump})|^2-m_0^2\right], \tag{5.44}$$

where $\Sigma_m=\Sigma_{m=m_0+M-1}^{m=m_0+M+1}$. From the distribution $\overline{P_M}(M)$, M is strongly peaked about $|M|\approx L_1$ for a jump of type J_1 and so this sum can be evaluated as

$$\begin{aligned}\delta E_{\rm tot}&\approx\frac{\hbar^2}{2m_ca^2}\left[(m_0\pm L_1)^2\sum_{\lambda,m}|\overline{c^M_{\lambda m}}(t^+_{\rm jump})|^2-m_0^2\right]\\ &\approx\frac{\hbar^2}{2m_ca^2}[(m_0\pm L_1)^2\overline{P_M}(L_1)-m_0^2],\end{aligned} \tag{5.45}$$

where the results of the normalization procedure in Appendix A 3 and summarized there by Eq. (A21) have been used. The $\pm$ means that $M=\pm L_1$ are equiprobable. After j such jumps the energy change is

$$\delta E_{\rm tot}(j)\approx\frac{\hbar^2}{2m_ca^2}\left[\left(\sum_\lambda\sum_{m=m_0+M^{\rm tot}(j)-j}^{m=m_0+M^{\rm tot}(j)+j}\times|\overline{c_{\lambda m}}(t^+_{\rm jump})|^2m^2\right)-m_0^2\right], \tag{5.46}$$

with $M^{\rm tot}(j)=\Sigma_{n_j=1}^{j}M(n_j)$ where $M(n_j)$ is the M value of the emitted photon at the n_jth jump as chosen randomly from $\overline{P_M}(M)$ at each jump. This can be evaluated approximately as

$$\delta E_{\rm tot}(j)\approx j\frac{\hbar^2}{2m_ca^2}L_1^2-[1-\overline{P_M}(L_1)]E_{\rm tot}(t=0), \tag{5.47}$$

since $\langle M^2\rangle\approx L_1^2$. Asymptotically, this scales linearly with j. This is easy to understand: a random walk in angular momentum $\mathbf{J}$ for j steps should give $\sigma^2_{\mathbf{J}}\sim j\Rightarrow\langle\delta E^{\rm free}_{\rm tot}(j)\rangle\sim j$. If $\sqrt{j}L_1$ is very large compared to m_0 then the number of orbits scales as

$$n_{\rm orbit}\sim\frac{\tau_{\rm heating}}{T_{\rm orbit}}\sim j^{3/2}\left(\frac{1}{s\Gamma(2\pi am_c/\hbar k^{\rm TM}_{P_1L_1})}\right). \tag{5.48}$$

The upper limit on the number of possible jumps j that the atom can undergo and still remain trapped is either the point at which the distribution in $\{m\}$ becomes peaked at such a large value $\sim\sqrt{j}L_1$ that the centrifugal force now matches the potential gradient, or when the bound state diffusion associated with these jumps [cf. Eq. (5.24) which implicitly shows a spreading from $\{\lambda\}$ to $\{\lambda'\}$ as well as from $\{m\}$ to $\{m'\}$] is enough to heat the atom. As pointed out earlier, the former would most likely dominate because heating by moving up the bound states ladder is suppressed due to the structure of $P_M(M)$.

VI. IMPLICATIONS OF THE QUANTIZATION OF THE c.m.

A. The atom-microsphere system as a matter wave resonator

The atom gallery system has the possibility of forming a matter wave resonator under certain conditions. To understand this requires resynthesizing the total c.m. wave function by including the ϕ dependence along with the c.m. bound states. Consider the full c.m. state under free evolution,

$$\begin{aligned}\langle \mathbf{r},t|\Psi^{\rm atom}_{\rm c.m.}\rangle&=\sum_{\lambda,m}c_{\lambda m}(t)\frac{u_\lambda(\rho,z)}{\sqrt{\rho}}e^{im\phi}\\ &=\sum_\lambda\left(\sum_m c_{\lambda m}(t)e^{im\phi}\right)\frac{u_\lambda(\rho,z)}{\sqrt{\rho}},\end{aligned} \tag{6.1}$$

and now concentrate on the spread in m values in $f_\lambda(t)=\Sigma_m c_{\lambda m}(t)e^{im\phi}$. It is easy to show that

$$\langle E(t)\rangle = \sum_{\lambda,m} |c_{\lambda m}(t)|^2 E_{\text{c.m.}}(\lambda) + \sum_{\lambda,m} |c_{\lambda m}(t)|^2 \frac{\hbar^2 m^2}{2m_c a^2}$$
$$= \langle E_{\text{c.m.}}(t)\rangle + \langle E_c(t)\rangle. \quad (6.2)$$

The de Broglie resonance condition is that $\Delta p_\phi \sim \hbar/a$ with $p_\phi(t) = \langle (\hbar/i\rho)(\partial/\partial\phi)\rangle \sim (\hbar/a)\Sigma_{\lambda,m} m|c_{\lambda m}(t)|^2$. Hence, $\Delta m \sim 1$ is required such that $\Sigma_{\lambda,m}$ contains very few m values. So with $\Delta m \sim 1$, $\Delta E_c \sim \hbar^2 m/m_c a^2$ defines an acceptable energy width and it is clear that with smaller diameter spheres, greater flexibility in initial atomic temperatures is allowed. For a 1 μm sphere at $E_c \sim 100$ nK (Cs recoil at the D_2 line at 852 nm), $\Delta E_c \sim (\hbar^2/m_c)(2\pi/a\lambda) \sim 30$ nK, which is not out of the question with present cooling and trapping technology. At this small radius, the Q of the microsphere is severely limited by its intrinsic radiative value, but the trapping potential does not depend heavily upon the Q. Previous discussions about the role of spontaneous emission in causing diffusion in the m quantum number of the c.m. wave function are particularly applicable here as the decohering mechanism and this will be the subject of a future investigation.

B. Cavity QED and the c.m. wave function

Perhaps the most interesting observation to come out of this analysis is that these c.m. wave packets have a spatial extent of $\lambda_{\text{optical}}/2\pi$. As has been alluded to previously, it is a very interesting problem to understand how such a c.m. wave packet would evolve if a quantum field were introduced. The idea of c.m. quantization in the context of cavity QED has recently been emphasized [40–42]. Interesting cavity QED effects arise when the atom is strongly coupled to a single mode of the field and it is necessary that the strong coupling parameter $g(\mathbf{r})$ between the atom and the privileged cavity mode (which is assumed to be at or near resonance with the atomic transition) dominate the decay rate Γ into all other modes and also the cavity decay rate κ of the privileged cavity mode. The atom gallery can realistically satisfy both these conditions as has been discussed in Ref. [2].

As a first example, we consider quickly turning off the classical trapping potential ($\Omega_{1,2} \to 0$) and then using the Stark shift of a quantum field resonant with a WGM and an internal atomic transition. The initial total wave function now contains a very well-defined initial atomic c.m. wave packet *localized directly in the spatial region of this quantum field* as pointed out in Ref. [2]. The quantum dynamics in a resonant situation such as this are governed by a Hamiltonian of the form

$$H = \frac{\mathbf{p}^2}{2m} + ig(\mathbf{r})(\sigma_- a^\dagger - \sigma_+ a), \quad (6.3)$$

where dissipation is ignored. The initial c.m. wave function,

$$|\Psi_{\text{c.m.}}(t=0)\rangle = |\Psi^{\lambda}_{\text{c.m.}}\rangle = \int d^3\mathbf{r} \left(\sum_{\lambda,m} c_{\lambda m} \frac{u_\lambda(\rho,z)}{\sqrt{\rho}} e^{im\phi} \right) |\mathbf{r}\rangle \quad (6.4)$$

forms a very realistic initial condition for the subsequent evolution and this situation is a novel one. Clearly, the usual interpretation of $g(\mathbf{r})$ as $g(\langle \mathbf{r}\rangle_\lambda)$ cannot be correct as the wave packet can have appreciable probability on spatial scales over which $g(\mathbf{r})$ varies appreciably.

Many very interesting situations may arise. For example, with $g(\mathbf{r}) \sim \mathbf{d}\cdot\mathbf{E}^{PLM}(\mathbf{r})$ (see Appendix A 4) for a quantized WGM field with mode functions given by Eq. (2.1), the c.m. wave function would be extremely sensitive to the number of nodes $|L-M|$ of $g(\mathbf{r})$ in the $\hat{\mathbf{e}}_z$ direction, because these determine how $g(\mathbf{r})$ varies across the wave packet (the realistic situation of a microsphere with some asphericity to lift the M degeneracy noted earlier is considered). This is emphasized in Figs. 16(a)–16(c) where the c.m. wave functions for the atom gallery modes $u_\lambda(\rho,z)$ are plotted along with $g^{|L-M|}(\rho,z)$ *on the same spatial scale*. For concreteness, the Cs D_2 transition is now taken to be close to resonant with a quantum WGM $(s,\mathbf{P}) = (\text{TM},1,521,M)$. In 16(a) and 16(b), $M = 518$ and in 16(c), $M = 517$. It is clear that the c.m. wave packets are not localized well enough to consider using $g(\langle \mathbf{r}\rangle_\lambda)$ in standard quantum dynamical equations for the internal states of the atom and the quantum field. Such a field would also lead to the importance of the coupling of the phase $e^{iM\phi}$ of $g(\mathbf{r})$ with the phase $e^{im\phi}$ of the c.m. wave function which is a concrete example for the discussion of Sec. V C.

A second possible avenue would be to take advantage of the long lifetime of these atom galleries and keep the trapping potential on while turning on a quantum field on a third transition. Unfortunately, the energy scale associated with the coupling parameters $g(\mathbf{r})$ for even a resonant vacuum field are $\sim 500\times$ greater than the dipole force potential for the cesium atom gallery calculated above. Hence, it is certainly not valid to assume that the atom will remain trapped while interacting with the quantum field. However, for a much lighter atom such as He*, it is the case that one might be able to treat the fast (g^{-1} time scales) dynamics due to the quantum field while ignoring the slower (heating time scales) of the trap. One could now consider the possibility of probing the c.m. state structure dependence of the usual internal state$\otimes$quantum field Jaynes-Cummings ladder in optical cavity QED on time scales long compared to anything being done at the moment. We look forward to developing these ideas further in future work.

VII. CONCLUSIONS

In conclusion, the atom gallery proposed in [2] has been further characterized by calculating the bound states and then examining the subsequent dynamics of the system evolving in one of these states. Trap lifetimes cannot be fully understood from a semiclassical analysis. Next, the broad issue of radiative processes in the atom gallery has been discussed in both the perturbative and nonperturbative regimes. The symmetry of the atom gallery brings to the fore very interesting issues of angular momentum conservation, which has been discussed in the context of the quantum jump picture. Some ideas about the atom gallery as a matter wave resonator have been presented. Finally, extremely interesting issues arise as a consequence of c.m. quantization in cavity QED with a quantum field. Exploring quantum dynamics against the

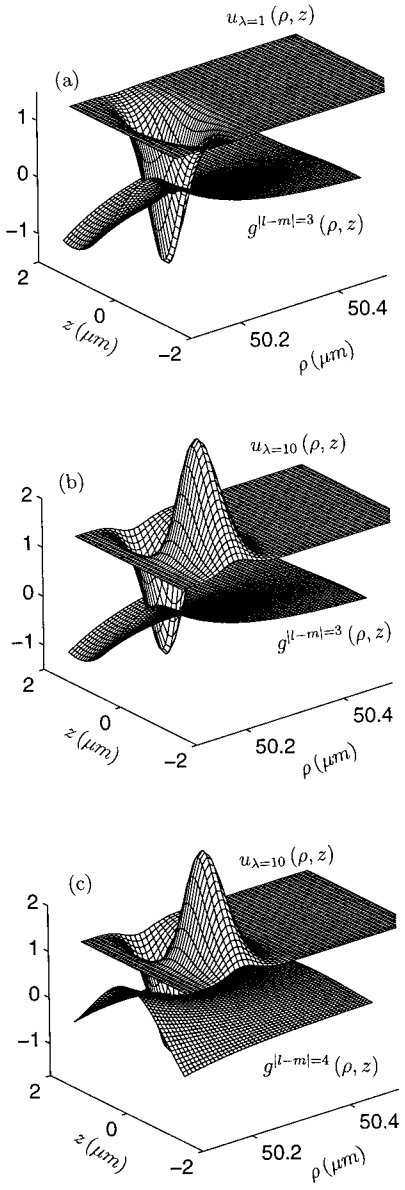

FIG. 16. The c.m. wave function $u_{\lambda=1}(\rho,z)$ is shown to have appreciable probability across the strong-coupling parameter $g^{|l-m|}(\mathbf{r})$ for the WGM (TM,p,l,m)=(TM,1,521,518) resonant with the cesium D_2 line at 852 nm, following the discussion in Sec. VI B. In (b), the same situation with the $u_{\lambda=10}(\rho,z)$ c.m. state is shown. In (c), the interesting situation arises that in the state $\lambda=10$ and with the WGM (TM,p,l,m)= (TM,1,521,517), then $g^{|l-m|=4}(\langle\mathbf{r}\rangle_{\lambda=10})\geqslant\langle g^{|l-m|=4}(\mathbf{r})\rangle_{\lambda=10}$ which emphasizes the importance of these c.m. wave functions when a quantum cavity field is involved on the same spatial scale. The understanding of this exciting new regime is one focus of our current work.

backdrop of the atom gallery should be extremely fruitful because it is a realistic 3D system which begins to emphasize the importance of the c.m. wave function in cavity QED.

ACKNOWLEDGMENTS

We express our gratitude to S. M. Tan for many of the codes used to implement the Lanczos algorithm and the invaluable aid concerning the use of MATLAB in the calculations. We also acknowledge many extremely helpful discussions with S. M. Tan and H. Mabuchi about atom galleries. The research was funded by the Office of Naval Research and by the National Science Foundation. D.W.V. acknowledges financial support from NSERC.

APPENDIX A: DETAILS ON THE CALCULATIONS

1. Microsphere resonances

a. Characteristic equations

Microsphere resonances are calculated from resonances in the Mie scattering coefficients which in turn are determined from the boundary conditions on Maxwell's equations at the surface of the sphere. For the TM modes used in the calculations the following characteristic equation has to be solved [11]:

$$\frac{[\rho j_L(\rho)]'}{n^2 j_L(\rho)}=\frac{\mu_2}{\mu_1}\frac{[(\rho/n)h_L^{(1)}(\rho/n)]'}{h_L^{(1)}(\rho/n)}, \tag{A1}$$

where n is the refractive index of silica, μ_1 and μ_2 are the magnetic permeabilities inside and outside the sphere, respectively, $\rho=k_1 a$ for a sphere of radius a and a wave vector magnitude inside the sphere of k_1, and the $'$ denotes differentiation with respect to the argument. This can be simplified to

$$\frac{j_{L-1}(\rho)}{j_L(\rho)}-\frac{L}{\rho}=\frac{nh_{L-1}^{(1)}(\rho/n)}{h_L^{(1)}(\rho/n)}-\frac{n^2 L}{\rho}. \tag{A2}$$

The solutions are characterized by ρ_{PL}^{TM} (where P indexes the zeroes of h_L) and are related to the resonance frequencies $\omega_{PL}^{\mathrm{TM}}=ck_{PL}^{\mathrm{TM}}/n$ used in the calculations by $\omega_{PL}^{\mathrm{TM}}=\mathrm{Re}(c\rho_{PL}^{\mathrm{TM}}/na)$. k_{PL}^{TM} is understood to be *inside* the sphere.

b. Quality factors

The cavity damping rate $\kappa_{PL}^{\mathrm{TM}}$ can be a *very* small number and this is the reason why microsphere resonators are interesting for strongly coupled cavity QED. In practice, the linewidths would be measured and quoted as a Q_{PL}^{TM}value, where $Q_{PL}^{\mathrm{TM}}=\omega_{PL}^{\mathrm{TM}}/\Delta\omega_{PL}^{\mathrm{TM}}=\omega_{PL}^{\mathrm{TM}}/2\kappa_{PL}^{\mathrm{TM}}$. This value can be predicted using the results of Ref. [31]. The intrinsic radiative Q can be solved by considering the functional form of the square of the Mie scattering coefficient b_L given explicitly for TM modes by Eq. (5.12). This leads to Q values which can be $>10^{20}$ for $2a/\lambda_{\mathrm{optical}}\geqslant 50$ (as is easily satisfied here) and so radiative losses can be ignored. Present work in Ref. [31] at 633 nm is pushing the intrinsic material absorption limit. For a typical Q value $\sim 10^9$ at $\lambda=894$ nm the resonance width is $\Delta\omega/2\pi\sim 300$ KHz, but a recoil shift here is ~ 10 KHz so these can be ignored as was claimed in Sec. V C 2.

2. Bound state calculations

a. Eigenvector representation

As discussed briefly above, the c.m. basis wave functions are held as coefficients of a sine series because this automatically enforces the boundary conditions that the atom be con-

fined to the well region. The sine series representation of $u_\lambda(\rho,z)$ can be written down explicitly as

$$u_\lambda(\rho,z)\rightarrow u_\lambda(\alpha,\beta) = \sum_{x=1}^{N_r}\sum_{y=1}^{N_z}\left[U_\lambda(x,y)\sin\left(\frac{\pi x\alpha}{N_r+1}\right)\sin\left(\frac{\pi y\beta}{N_z+1}\right)\right], \tag{A3}$$

and the variables ρ and z have been discretized as

$$\rho=\rho_{\min}+\frac{\alpha}{N_r+1}(\rho_{\max}-\rho_{\min}), \qquad z=z_{\min}+\frac{\beta}{N_z+1}(z_{\max}-z_{\min}), \tag{A4}$$

with $\alpha=1,\ldots,N_r$, $\beta=1,\ldots,N_z$. N_r,N_z are the grid sizes in the $\hat{\mathbf{e}}_\rho$ and $\hat{\mathbf{e}}_z$ directions, respectively, for which $N_r=N_z=40$ was chosen. $U_\lambda(x,y)$ is known as the *2D Inverse sine transform* of $u_\lambda(\alpha,\beta)$. The complementary relation reads

$$U_\lambda(x,y)=\frac{4}{(N_r+1)(N_z+1)}\sum_{\alpha=1}^{N_r}\sum_{\beta=1}^{N_z} \times\left[u_\lambda(\alpha,\beta)\sin\left(\frac{\pi x\alpha}{N_r+1}\right)\sin\left(\frac{\pi y\beta}{N_z+1}\right)\right], \tag{A5}$$

and $u_\lambda(\alpha,\beta)$ is the *2D sine transform* of $U_\lambda(x,y)$. The coefficients $U_\lambda(x,y)$ and $u_\lambda(\alpha,\beta)$ are purely real and they obey

$$\sum_{\alpha,\beta}u_\lambda^2(\alpha,\beta)=\frac{(N_r+1)(N_z+1)}{4}\sum_{x,y}U_\lambda^2(x,y). \tag{A6}$$

There is still the issue of the overall normalization of the $u_\lambda(\alpha,\beta)$, because

$$\int d^3\mathbf{r}\Psi_{\text{c.m.}}^{\text{atom}*}(\rho,\phi,z,t)\Psi_{\text{c.m.}}^{\text{atom}}(\rho,\phi,z,t)=1. \tag{A7}$$

This equation can be rewritten as

$$\int d^3\mathbf{r}\left[\left(\sum_{\lambda',m'}c_{\lambda'm'}^*\frac{u_{\lambda'}(\rho,z)}{\sqrt{\rho}}e^{-im'\phi}\right) \times\left(\sum_{\lambda,m}c_{\lambda m}\frac{u_\lambda(\rho,z)}{\sqrt{\rho}}e^{im\phi}\right)\right]=1. \tag{A8}$$

The ϕ integration gives $2\pi\delta_{m',m}$ and so

$$2\pi\sum_{\lambda,\lambda',m}c_{\lambda'm}^*c_{\lambda m}\int\rho d\rho dz\frac{u_{\lambda'}(\rho,z)u_\lambda(\rho,z)}{\rho}=1. \tag{A9}$$

Now evaluating the integral gives

$$I=\int\rho d\rho dz\frac{u_{\lambda'}(\rho,z)u_\lambda(\rho,z)}{\rho}=\delta_{\lambda',\lambda}\int\rho d\rho dz\frac{u_\lambda^2(\rho,z)}{\rho}, \tag{A10}$$

because the $\{u_\lambda(\rho,z)\}$ are eigenfunctions of a Hermitian operator and hence are orthogonal. Using Eqs. (A3) and (A4),

$$I=\delta_{\lambda',\lambda}\frac{(\rho_{\max}-\rho_{\min})(z_{\max}-z_{\min})}{4}\sum_{x,y}U_\lambda^2(x,y). \tag{A11}$$

The end requirement is

$$\frac{\pi}{2}(\rho_{\max}-\rho_{\min})(z_{\max}-z_{\min})\sum_{\lambda,m}c_{\lambda m}^*c_{\lambda m}\sum_{x,y}U_\lambda^2(x,y)=1. \tag{A12}$$

To independently normalize the $\{u_\lambda(\rho,z)\}$, it is required that

$$\sum_{x,y}U_\lambda^2(x,y)=\frac{2}{\pi(\rho_{\max}-\rho_{\min})(z_{\max}-z_{\min})}, \tag{A13}$$

and then the expansion coefficients must obey

$$\sum_{\lambda,m}c_{\lambda m}^*c_{\lambda m}=1. \tag{A14}$$

Thus the proper way to normalize the $\{u_\lambda(\rho,z)\}$ is to have

$$\sum_{\alpha,\beta}u_\lambda^2(\alpha,\beta)=\frac{(N_r+1)(N_z+1)}{2\pi(\rho_{\max}-\rho_{\min})(z_{\max}-z_{\min})}. \tag{A15}$$

The power of this method is clear when the Schrödinger equation, Eq. (3.2), is examined. First, the second derivative operator just becomes a multiplication of $U_\lambda(x,y)$ by $-\pi^2x^2/(\rho_{\max}-\rho_{\min})^2-\pi^2y^2/(z_{\max}-z_{\min})^2$. Second, it is very *fast* to switch between $u_\lambda(\rho,z)$ and $U_\lambda(x,y)$ using modifications of 2D fast fourier transform (FFT2) algorithms to the 2D fast sine transform (FST2).

3. Renormalization of the wave function and the quantum jump probability density

It is necessary to renormalize the distribution $P_M(M)$ according to

$$P_M(M)\rightarrow\overline{P_M}(M)=\mathcal{K}P_M(M), \tag{A16}$$

where

$$\sum_{M'}\overline{P_M}(M')=1, \tag{A17}$$

so that

$$\mathcal{K}\sum_{\lambda'm'}|c_{\lambda'm'}^{M'}|^2=1. \tag{A18}$$

In order to renormalize $\langle\mathbf{r},t|\Psi_{\text{tot}}^{\text{system}}\rangle$ after the jump,

$$c_{\lambda'm'}^{M'}\rightarrow\overline{c}_{\lambda'm'}^{M'}=\mathcal{M}c_{\lambda'm'}^{M'}, \tag{A19}$$

such that

$$\sum_{\lambda'm'}|\overline{c}_{\lambda'm'}^{M'}|^2=1. \tag{A20}$$

Finally, then, the relationship between the required normalizations is

$$\mathcal{K}=|\mathcal{M}|^2. \tag{A21}$$

4. Coupling coefficients and photon numbers

If the microsphere is to be used in the regime of strong coupling, the parameter of interest is the coupling coefficient $g_{s,\mathbf{p}}(\mathbf{r})$ where [35]

$$g_{s,\mathbf{p}}(\mathbf{r})=\gamma_\perp|\psi_{s,\mathbf{p}}(\mathbf{r})|\sqrt{\frac{3c\lambda^2}{4\pi\gamma_\perp V_{s,\mathbf{p}}}}. \tag{A22}$$

and $\gamma_\perp$ is the *free space* transverse decay rate for the internal atomic transition of frequency $\omega_{\rm int}^{\rm atom}=2\pi c/\lambda_{\rm atom}$. These are easily calculated using the definitions of $V_{s,\mathbf{p}}$, $\psi_{s,\mathbf{p}}(\mathbf{r})$, and

$$\gamma_\perp=\frac{1}{2}\Gamma^{\rm free}(\lambda)=\frac{4e^2X_R^2\pi^2}{3\hbar\lambda^3}. \tag{A23}$$

The photon numbers are calculated from $\Omega_{1,2}(\mathbf{r})=2\sqrt{\langle n_{1,2}\rangle}g_{s,\mathbf{p}}(\mathbf{r})$. It is also interesting to note that the discussion in Sec. VI B addresses a situation in which the phase of $g_{s,\mathbf{p}}(\mathbf{r})$ may mix with the phase of the c.m. wave function so that the typical definition of $g_{s,\mathbf{p}}(\mathbf{r})$ which includes the norm of the radiation field mode function $|\psi_{s,\mathbf{p}}(\mathbf{r})|$ [as in Eq. (A22)] would have to be modified.

[1] H. Wallis, J. Dalibard, and C. Cohen-Tannoudji, Appl. Phys. B **54**, 407 (1992); M. Holland, S. Marksteiner, P. Marte, and P. Zoller, Phys. Rev. Lett. **76**, 3683 (1996).

[2] H. Mabuchi and H. J. Kimble, Opt. Lett. **19,** 749 (1994).

[3] M. L. Gorodetsky and V. S. Ilchenko, Opt. Commun. **113**, 133 (1994); J. C. Knight, N. Dubreuil, V. Sandoghar, J. Hare, V. Lefèvre-Seguin, J. M. Raimond, and S. Haroche, Opt. Lett. **20**, 1515 (1995); **21**, 698 (1996).

[4] F. Treussart, J. Hare, L. Collot, V. Lefèfvre, D. S. Weiss, V. Sandoghdar, J. M. Raimond, and S. Haroche, Opt. Lett. **19**, 1651 (1994).

[5] K. S. Wong, M. J. Collett, and D. F. Walls (unpublished).

[6] W. Jhe and J. W. Kim, Phys. Rev. A **51**, 1150 (1995).

[7] H. Chew, J. Chem. Phys. **87**, 135 (1987).

[8] V. V. Klimov and V. S. Letokhov, Opt. Commun. **122,** 155 (1996).

[9] V. V. Klimov, M. Ducloy, and V. S. Letokhov, J. Mod. Opt. **43**, 549 (1996).

[10] V. B. Braginsky, M. L. Gorodetsky, and V. S. Ilchenko, Phys. Lett. A **137**, 393 (1989).

[11] J. A. Stratton, *Electromagnetic Theory* (McGraw-Hill, New York, 1941), p. 554.

[12] *Handbook of Laser Science and Technology, Vol. 3*, edited by M. J. Weber (CRC Press, Boca Raton, 1982), Pt. 1.

[13] J. D. Miller, R. A. Cline, and D. J. Heinzen, Phys. Rev. A **47**, R4567 (1993).

[14] C. Cohen-Tannoudji, J. Dupont-Roc, and G. Grynberg, *Atom-Photon Interactions* (Wiley, New York, 1992).

[15] M. Chevrollier, M. Fichet, M. Oria, G. Rahmat, D. Bloch, and M. Ducloy, J. Phys. (France) II **2,** 631 (1992).

[16] S. M. Tan (private communication).

[17] J. P. Dowling and J. Gea-Banacloche, Adv. At. Mol. Opt. Phys. (to be published).

[18] J. K. Cullum and R. A. Willoughby, *Lanczos Algorithms for Large Symmetric Eigenvalue Computations, Vol. I and Vol. II* (Birkhäuser, Stuttgart, 1985).

[19] D. A. Varsalovich, A. N. Moskalev, and V. K. Khershonskii, *Quantum Theory of Angular Momentum* (World Scientific, Singapore, 1988), p. 130.

[20] R. Kosloff, J. Phys. Chem. **92**, 2087 (1988).

[21] J. Dalibard and C. Cohen-Tannoudji, J. Opt. Soc. Am. B **2**, 1707 (1985); C. Cohen-Tannoudji, in *Fundamental Systems in Quantum Optics*, Les Houches Summer School Session LIII, edited by J. Dalibard, J. M. Raimond, and J. Zinn-Justin (Elsevier, Amsterdam, 1992), p. 49; J. P. Gordon and A. Ashkin, Phys. Rev. A **21**, 1606 (1980).

[22] H. J. Carmichael, *An Open Systems Approach to Quantum Optics* (Springer-Verlag, New York, 1993); C. W. Gardiner, A. S. Parkins, and P. Zoller, Phys. Rev. A **46**, 4363 (1992); K. Molmer, Y. Castin, and J. Dalibard, J. Opt. Soc. Am. B **3**, 524 (1993).

[23] S. Haroche and D. Kleppner, Phys. Today **42** (1), 24 (1989).

[24] S. Haroche, in *Fundamental Systems in Quantum Optics*, Les Houches Summer School Session LIII, edited by J. Dalibard, J. M. Raimond, and J. Zinn-Justin (Elsevier, Amsterdam, 1992), p. 771.

[25] E. A. Hinds, in *Advances in Atomic, Molecular and Optical Physics*, edited by D. Bates and B. Bederson (Academic, New York, 1990), Vol. 87, p. 325.

[26] K. Rzazewski and W. Zakowicz, J. Phys. B **25**, L319 (1992).

[27] O. Steuernagel and H. Paul, Phys. Rev. A **53**, 2983 (1996).

[28] H. Chew, D.-S. Wang, and M. Kerker, Appl. Opt. **18,** 2679 (1979); J. S. Kim and S. S. Lee, J. Opt. Soc. Am. **73,** 303 (1983).

[29] P. D. Drummond, IEEE J. Quantum Electron. **QE-17**, 301 (1981).

[30] D. Kleppner, Phys. Rev. Lett. **47**, 233 (1981).

[31] M. L. Gorodetsky, A. A. Savchenkov, and V. S. Ilchenko, Opt. Lett. **21**, 453 (1995).

[32] L. Collot, V. Lefèvre-Seguin, M. Brune, J. M. Raimond, and S. Haroche, Europhys. Lett. **14**, 19 (1991).

[33] H. Mabuchi, D. W. Vernooy, and H. J. Kimble (unpublished).

[34] *Optical Effects Associated with Small Particles*, edited by P. W. Barber and R. K. Chang (World Scientific, Singapore, 1988).

[35] H. J. Kimble, in *Cavity Quantum Electrodynamics, Advances in Atomic, Molecular and Optical Physics, Supplement 2*, edited by P. R. Berman (Academic, San Diego, 1994).

[36] P. Marte, R. Dum, R. Taïeb, and P. Zoller, Phys. Rev. A **47,** 1378 (1993); P. Marte, R. Dum, R. Taïeb, P. D. Lett, and P. Zoller, Phys. Rev. Lett. **71**, 1335 (1993).

[37] V. C. M. De Witt and J. H. D. Jensen, Z. Naturforsch. Teil A **8**, 267 (1953).
[38] S. J. van Enk, Quantum Opt. **6**, 445 (1994).
[39] C. W. Gardiner and P. Zoller (unpublished).
[40] M. O. Scully, G. M. Meyer, and H. Walther, Phys. Rev. Lett. **76**, 4144 (1996).
[41] W. Ren and H. J. Carmichael, Phys. Rev. A **51**, 752 (1995).
[42] S. Haroche, M. Brune, and J. M. Raimond, Europhys. Lett. **14**, 19 (1991).